ELECTROSPINNING COLLAGEN AND HYALURONIC ACID NANOFIBER MESHES

A Thesis Presented to

the Faculty of the Graduate School

at the University of Missouri

In Partial Fulfillment

Of the Requirements for the Degree

Master of Science

By

RACHAEL FISCHER

Dr. Sheila Grant, Thesis Supervisor

DECEMBER 2011

The undersigned, appointed by the dean of the Graduate School, have examined this thesis entitled

ELECTROSPINNING COLLAGEN AND HYALURONIC ACID NANOFIBER MESHES

Presented by Rachael Fischer,

a candidate for the degree of Master of Science,

and hereby certify that, in their opinion, it is worthy of acceptance.

Dr. Sheila Grant, Biological Engineering Department

Dr. Heather Hunt, Biological Engineering Department

Dr. Derek Fox, Department of Veterinary Medicine and Surgery

To God, I can do all things through him who gives me strength, Philippians 4:13.

To my parents, Dr. Anthony Fischer and Shelly Zumsteg, who showed me how to love, taught me the importance of education, always encouraged me to pursue my dreams, and supported me in immeasurable ways throughout it all.

To my twin sister Leslie, my best friend, your strength and courage through the past few years is a daily motivation to work hard and be thankful for the many blessings I have been given.

To my grandfather, Donald Zumsteg, you were a lifelong teacher and will truly be missed. To my grandmother, Anne Zumsteg, your life experiences are what led me to become a biomedical engineering.

To my friends, I never would have made it this far without all of your love and support. Thanks for making me laugh so hard I cry and for helping me to enjoy life always!

ACKNOWLEDGEMENTS

First and foremost, I am heartily thankful to my supervisor, Dr. Sheila Grant, for allowing me the opportunity to conduct my graduate research under her guidance. As an undergraduate student, I had the opportunity to take her classes as well as perform research in her lab where I gained a passion for biomedical engineering. Her willingness to teach and assist all students has motivated me to continue in research and pursue this advanced degree.

In addition to Dr. Grant, I would like to acknowledge and thank my other committee members, Dr. Heather Hunt and Dr. Derek Fox, for providing invaluable feedback on my research. I would also like to recognize Dr. Mohamed Khalid who developed the concept for this project and assisted in the initial brainstorming of the research objective and project constraints.

I am truly indebted and thankful for my undergraduate research assistant, Michael McCoy, for his support throughout the entire research process. His assistance with many of the experiments was vital to their success and his willingness to contribute did not go unnoticed.

Additionally, I would like to express my gratitude to Matt Cozad whose knowledge of the lab equipment and guidance was instrumental throughout my research process. I also offer my regards to the other members of the lab for creating a fun and inviting research environment. Lab meetings and long hours in the lab would not have been the same without all of you.

Lastly, I would like to thank the University of Missouri and the College of Engineering for creating an institution with an atmosphere that is conducive for research.

TABLE OF CONTENTS

LIST OF FIGURES

LIST OF TABLES

ELECTROSPINNING COLLAGEN AND HYALURONIC ACID NANOFIBER MESHES

Rachael Fischer

Dr. Sheila Grant, Thesis Supervisor

ABSTRACT

Osteoporosis is a worldwide burden affecting over 200 million people. There are many risk factors associated with osteoporosis, but they all lead to decreased bone strength and an increased chance of bone fracture. The field of tissue engineering could be used to create bone substitute materials that can increase bone strength or promote new bone growth. Collagen and hyaluronic acid (HA) are particularly interesting due to their roles in the extracellular matrix (ECM) of humans and their ability to stimulate bone forming cells. These materials can be processed into nanofiber scaffolds using a technique called electrospinning; a process that applies high voltage to a polymer solution to draw out nanofibers that are collected on a ground plate. An electrospinning solution of collagen/HA was synthesized, and the electrospinning apparatus was adjusted to generate uniform nanofiber meshes with consistent nanofiber diameter. The meshes were then crosslinked to render them insoluble in aqueous solutions, and gold nanoparticles (AuNPs) were conjugated to the surface to promote cellular in-growth. Scanning electron microscope (SEM) was utilized to image the nanofiber mesh surface and electron dispersive spectroscopy (EDS) was used to quantify the charged particles on the mesh as gold. Fourier transform infrared spectroscopy (FT-IR) was used to find the absorption spectrum and bonding changes after each step. A WST-1 assay was also performed to determine the potential biocompatibility. The results show that it was possible to develop scaffolds that were insoluble in aqueous solutions and promoted cellular attachment and proliferation. In conclusion, nanofiber meshes made from collagen/HA could be utilized as a tissue engineered scaffold to promote bone growth.

CHAPTER 1
OSTEOPOROSIS AND BONE FORMATION

1.1. Introduction to Osteoporosis

1.1.1. *Osteoporosis Causes and Risk Factors*

As baby boomers continue to age, many new health problems are becoming of high concern due to their ability to limit the quality of life of an individual. Additionally, health care costs are rising and the aging population is interested in learning about innovative treatment methods that not only treat a problem, but also help prevent future complications. One health concern that is becoming an increasing worldwide burden is the disease known as osteoporosis which affects over 200 million people worldwide (WHO 2004). As a result of this disease, in the year 2000 alone there were an estimated 9 million osteoporotic related fractures of which 1.6 million were in the hip (Johnell and Kanis 2006). It can be assumed that similar occurrences happen on a yearly basis which is why the incidence of a fracture due to osteoporosis is such a major health concern. Osteoporosis is defined as a disease that is characterized by low bone mass and micro-architectural deterioration of bones, leading to fragile bones and an increased risk of bone fracture (Hosoi 2010; Kaveh et al. 2010; Ritchie 2010). This definition is based on bone mineral density (BMD), which is the amount of bone mineral per unit cross sectional area, and is the standard indicator of bone health (Hosoi 2010; Kaveh et al. 2010).

There are many biological and environmental factors that influence a person's BMD and their predisposition to osteoporosis (Hosoi 2010; Ritchie 2010). These factors include age, gender, mechanical loading, nutrition, genes, and the skeletal site of the

bone. A combination of many of these factors often leads to osteoporosis, where over time, the amount of bone needed for mechanical support drops below a certain necessary threshold and a fracture may occur (Kaveh et al. 2010). Having osteoporosis does not guarantee a fracture; it only means there is a decreased BMD with an increased fracture risk. By looking more closely at the risk factors that cause osteoporosis, a deeper understanding of the disease can be achieved.

Age and gender are the most commonly studied areas in determining the risk of having osteoporosis. In particular, aging women have the highest chance of getting osteoporosis and experiencing many of its side effects. Age is a factor because bone components such as collagen begin to deteriorate with age, which disturbs the bone remodeling environment and decreases the overall strength of bone (Ritchie 2010). Gender is also a factor because systemic hormones regulate osteoblastic and osteoclastic cellular activities (Kaveh et al. 2010). The importance of these two cells will be detailed in the next section; however, they are vital to the formation of strong bones. In women, estrogen deficiency in particular increases the lifespan of osteoclasts, the bone resorbing cell, and reduces the lifespan of osteoblasts, the bone forming cell, which causes a net decrease in bone mass leading to osteoporosis (Kaveh et al. 2010; Seeman 2008).

Mechanical loading also affects bone strength and can have compound effects when combined with age and gender. Human bodies are variable and change based on physical needs that must be met. Regular mechanical loading, such as weight lifting and an active life style, will encourage an increased BMD and a decreased risk of osteoporosis. This is because bones develop to support one's level of activity. A more active individual will generate stronger bones because the body needs them to support the stresses and strains activity requires. Age affects an individual's bone density

because as one ages they become less active, which leads to less load being placed on various bones. This causes an overall decreased bone strength due to their adaptation to a more sedentary life style (Kaveh et al. 2010; Ritchie 2010). Gender effects of mechanical loading can be seen by comparing the skeletal system of men and women. In general, men have a larger skeleton which produces stronger bones that can tolerate larger loads (Seeman 2008). Women on the other hand, have smaller bones which are weaker because they are not developed to support large loads. In turn, the reduced BMD leads to an increased risk of osteoporosis.

Nutrition is also important because if proper vitamins and minerals are not received through a balanced diet or supplements, the body will try to meet needs by using other vitamin and mineral storage areas such as bones, making them weaker. In particular, calcium, vitamin D, and vitamin K are all important to promote strong and healthy bones (Hosoi 2010; Reid et al. 2008; WHO 2004). These are also common supplements that can be taken in order to ensure that dietary needs are met. Their importance will be discussed in more detail in the current treatment and prevention section.

Genes and family history are also important factors in determining ones chance of having osteoporosis. Like many diseases, when other close family members are affected it is most likely passed onto future generations (Hosoi 2010; Pocock et al. 1987). The reason for this is attributed to genes and one's predisposition to having a low BMD. This is also why some men have higher chances of getting osteoporosis, and some postmenopausal women are not affected. Early studies compared the BMD of different regions of the body among both fraternal and identical twins. The findings showed that twin sets had similar BMD throughout the body, with the largest relation

being in the spine. The forearm and hip had less similarities due to lifestyle factors that have a larger effect on these regions (Pocock et al. 1987).

Hosoi (2010) recently looked more closely at the human genome to try and find genetic links to osteoporosis and low BMD. One gene that was studied was the tissue-nonspecific alkaline phosphatase (TNSALP) gene that is in the plasma membrane of osteoblasts, the bone forming cell that supplies phosphate to the calcification site. One particular exon, *787 His*, was shown to encourage more efficient calcification and therefore result in a higher BMD, as opposed to the *787 Try* exon, which may not improve calcification. Other genes associated with vitamin D and vitamin K regulation were also studied, where it was seen that the regulation and utilization of these essential vitamins could be controlled genetically and could affect one's BMD (Hosoi 2010). This shows that there are many genetic factors that could alter one's chance of getting osteoporosis, that are independent of environment and lifestyle.

The skeletal site of the bone also affects its risk of osteoporosis and possible fracture. The most common fracture sites for osteoporotic breaks are the forearm, vertebrae, and hip (Gauthier et al. 2011; Johnell and Kanis 2006; WHO 1992, 2004). Table 1.1 shows the percent chance of getting a bone break in the common fracture sites divided among men and women. From this, it is clear that women are much more susceptible to all three fracture types. Forearm fractures are often the result of falling onto an outstretched hand. This type of fracture does not normally require hospitalization and has a low resulting morbidity when compared to other fracture types, but it can still be very painful and does require some medical treatment. A forearm fracture is uncommon in men, but it is estimated that up to 20% of 70 year old women will have experienced a wrist fracture. Vertebral fractures are often hard to classify because this fracture is often asymptomatic. In some cases there is back pain, but it is usually too

minimal to investigate the effects. The medical costs are also often low, because they do not require medical attention. Hip fractures are often the most severe and often occur from falling. This fracture type causes hospitalization, surgery, and has a high rate of morbidity. It is often very painful and recovery can be slow, since decreased movement causes additional bone loss and a decreased quality of life. There is also a high economic cost to a hip fracture because of medical bills, hospital stays, and the high chance of recurrence or additional fractures (WHO 1992).

Table 1.1: Estimated lifetime fracture risk after age 50 (WHO 1992)

Fracture Site	Women (%)	Men (%)
Hip	17.5	6.0
Vertebra	15.6	5.0
Forearm	16.0	2.5
Any of the above	**39.7**	**13.1**

In conclusion, it is evident that many of these factors are interrelated. This means that trying to generate a treatment for one factor alone may only delay the onset of osteoporosis because the effects of other risk factors will eventually evolve. Environmental factors such as mechanical loading and nutrition can be individually monitored by making lifestyle changes to reduce the risk of osteoporosis by maintaining a healthy lifestyle. Biological factors like gender and genes cannot be altered, and when the undeniable effect of aging set in, osteoporosis becomes a very multidimensional disease requiring complex treatments that are currently unavailable.

1.1.2. *Postmenopausal Osteoporosis*

As mentioned previously, there are many risk factors associated with the disease osteoporosis. Two of these are age and gender. These are important factors because a large percentage of people with osteoporosis are postmenopausal women (Gauthier et al. 2011). The World Health Organization did a study in the early 1990s to determine what percentage of women had osteoporosis. Their results are summarized in Table 1.2. The study defined osteoporosis as a BMD of more than 2.5 standard deviations below a young adult reference at the same site (WHO 1992). This study shows that women start to become susceptible in their 50s when menopause normally occurs. Then as they continue to age and age related factors combine with postmenopausal hormone deficiencies their risk continues to increase.

Table 1.2: Percentage of white women with osteoporosis (WHO 1992)

Age range	Osteoporosis of	
	Any site (%)	Hip alone (%)
30-39	0	0
40-49	0	0
50-59	14.8	3.9
60-69	21.6	8.0
70-79	38.5	24.5
80+	70.0	47.5

Other studies have found that 3-6% of women will have osteoporosis at the age of 50 and that percentage will rise to 50-75% by the age of 90. In addition, the risk of a fracture due to osteoporosis in women over 50 is 30-40% (Gauthier et al. 2011; WHO 2004). In order to quantify the risk of fractures, one group developed a postmenopausal

osteoporosis model based on data and extrapolated out to the year 2020. Population data was taken from women in Sweden from 1970 to 2007 and future data was forecast based on rising life expectancy and rising populations reaching postmenopausal age. The model predicts that the number of women experiencing a fracture due to osteoporosis between 2009 and 2020 will increase by 11.5%. More specifically, the number of women experiencing a hip fracture due to osteoporosis will increase by 7.7% (Gauthier et al. 2011). Worldwide data shows that in 2000 61% of all fractures occur in women, and 70% of hip fractures occur in women. More specifically, there were 490 thousand hip fractures in men and 1,137 thousand hip fractures in women in the year 2000 showing that osteoporotic fractures occur in both men and women, but are far more prevalent in women (Johnell and Kanis 2006).

1.1.3. *Current Treatments*

Knowing the risk factors for osteoporosis is an important first step in determining possible susceptibility to the disease. From there, prevention actions can be taken by those who are unaffected by osteoporosis, and treatment methods can be implemented for those who may already be experiencing the effects of osteoporosis. In order to help reduce several of the risk factors of osteoporosis, and to promote good bone health, several treatments are available. These include dietary supplements, hormone replacement therapy (HRT), or prescription drugs made to target certain cells or interactions related to bone health (Cleland et al. 2010; Kaveh et al. 2010). The easiest treatment would be personal prevention by limiting as many of the risk factors as possible. This could include being active, eating healthy, and being aware of the effects age could have on the skeletal system. Additionally, vitamin supplements, such as calcium and vitamin D, could be beneficial to help prevent bone loss. This is most

important in postmenopausal women who are known to be calcium deficient. HRT such as estrogen, calcitonin and biophosphonate could also help promote stronger bones. Estrogen therapy is most effective when it begins just after menopause and has been shown to help maintain a healthy BMD. Calcitonin and Biophosphates are both used to inhibit bone resorption by osteoclast function. There are also several medications available to promote osteoblasts and new bone formation. Sodium fluoride drugs increase trabecular bone mass. Parathyroid therapy and strontium ranelate can also help promote new bone formation (Cleland et al. 2010; Kaveh et al. 2010).

Kaveh et al. (2010) and Cleland et al. (2010) explain that using these treatment methods could cause unforeseen side effects or might not be as effective in reducing fracture as first thought. For example some sodium fluoride treatments have been seen to decrease cortical bone mass, even though they effectively increase trabecular bone mass (Kaveh et al. 2010). There have also been many studies that show that calcium and vitamin D supplementation do increase bone mass, but not enough to reduce the risk of osteoporotic fracture. (Cleland et al. 2010). Some studies that do show positive results have many problems such as small sample size and a short testing period. Part of this could be due to the long list of risk factors that lead to osteoporosis but are hard to accurately measure. Collecting strong data would also involve long term studies that measure bone mass over 30 or more years, which is not plausible in most cases. Additionally, continual use of many of the therapies is needed for them to be effective; however, this can often be expensive for patients and still have variable results. In a study of many treatment methods, the most effective treatment was hormone therapy treatments consistently administered for at least one year (McCombs et al. 2004).

These treatment and prevention methods can help reduce risk fractures and promote cells that can influence bone growth, but they lack the ability to specifically add new bone material. Bone is very complex, and drug treatment alone is not always enough to eliminate the chance of getting osteoporosis, which is evident in the number of people affected. Additionally, calcium provides strength to bone in compression, but does not provide strength to bone in tension or undergoing stretching (Lujan and White 2011). This means that some of the treatment methods are only addressing compressive bone strength, and not strength in tension. By taking a closer look at the formation of bone itself, it could be possible to introduce new bone components directly to the bone network that could help prevent osteoporosis and related fractures.

1.2. Introduction to Bone Formation

1.2.1. Bone Formation Pathway

Bones are vital to the support and structure of the human body. The skeletal system is constantly rebuilding and remodeling itself based on the bone formation pathway. This pathway is affected by nutrients in our blood stream as well as an individual's lifestyle. Bone strength is maintained to support one's daily activity level and is constantly changing to adapt to an individual's environment. In addition to the normal rebuilding cycle, remodeling may be triggered if micro-cracks form due to increased stresses or strains on the bone that could be the result of a minor injury or fall (Bartel et al. 2006; Seeman 2008; Seeman and Delmas 2006).

The bone formation pathway carefully pairs bone resorption with new bone formation and can be seen in Figure 1.1. There are many different cell types that are contribute to this pathway and they include: osteocytes, bone lining cells, osteoblasts, and osteoclasts. Osteocytes are the most numerous cell and are osteoblasts that

become imbedded within the bone. They are connected by channels called canaliculi which provide the proper nutrients and signaling pathway. When a microcrack occurs, the canaliculi is severed and this signaling pathway is broken causing osteocyte apoptosis. This signals to bone lining cells that remodeling needs to take place. The bone lining cells, which are flattened osteoblasts, release local factors that signal where and how much bone needs to be reabsorbed. These factors trigger osteoclasts, to resorb the bone. This then triggers osteoblasts to form new bone which then differentiate into a more specific cell type based on their location (Bartel et al. 2006; Seeman 2008).

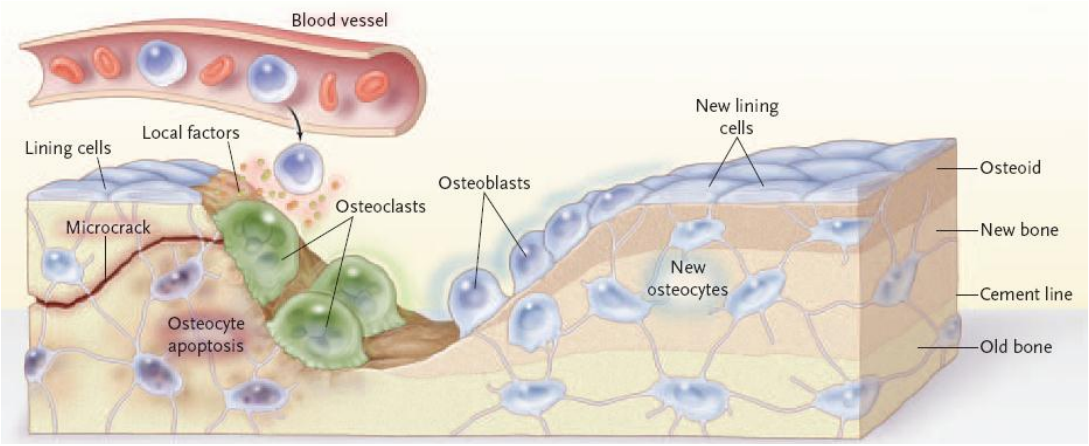

Figure 1.1: Bone formation pathway (Seeman and Delmas 2006)

1.2.2. Bone Composition

Bone is very unique and must exhibit many different characteristics. It needs to be stiff and resist deformation to make loading possible. It also needs to be flexible and absorb energy by deforming. This flexibility must allow bone to shorten and widen in compression and lengthen and narrow in tension. In addition, it must be light weight so it does not hinder an individual's movement yet it must maintain enough strength to

support the other systems in the body (Bartel et al. 2006; Seeman 2008). This ability to be stiff and flexible, and light and strong is achieved by bone's distinctive composition.

Bone is composed of a unique set of materials that include both organic and inorganic phases. The organic phase is 90% type I collagen and 10% amorphous ground substance that include collagen II, collagen III, and the non-collagen proteins including osteocalcin, osteonectin, and osteopontin. The inorganic phase consists of calcium hydroxyapatite (Bartel et al. 2006; Ritchie 2010; Seeman 2008). Based on weight distribution bone is 60% organic, 30% inorganic, and 10% water and based on volume bone is 40%, 35%, and 2.5% of the previous components, respectively. The most important ingredient is the collagen because it is the most abundant protein in the body. Collagen is made up of three amino acid chains that form a triple helix, termed a tropocollagen molecule. Several collagen fibers form fibril arrays that are connected by the organic phase and provide a structure for the cellular components of bone. The fibrils then arrange themselves in either stacked sheets called lamellae or blocks of randomly oriented fibers. The arrangement of these fibers then distinguishes itself into a specific form of bone tissue (Bartel et al. 2006; Ritchie 2010).

There are two main types of bone tissue: trabecular bone and cortical bone. Part of bone's uniqueness is this tissue structure, which is selected based on the bone type, and location of the tissue within each individual bone. Trabecular bone, also known as cancellous bone, is located on the inside of the bone, and has a spongy appearance with small micrometer size holes throughout. Cortical bone, also known as compact bone, is much denser, and is located on the surface of all bones (Bartel et al. 2006; Ritchie 2010). There are several distinct differences between these tissue types. Cortical bone is arranged around Haversian canals, which consist of many layers of lamellar bone. At the center of the canal there are blood vessels, capillaries, and many bone

cells. This allows the bone to sense micro-cracks and signal when new bone needs to be formed. Trabecular bone has a more open cellular structure unlike the Haversian cortical bone. This makes signaling the bone formation pathway more difficult, but it is still known to adapt and regenerate when faced with large deformations (Bartel et al. 2006).

The bone formation pathway is complex and constantly changing based on nutrition, activity level, and age. These factors along with gender, genes, and mechanical loading also contribute to the risk of osteoporosis. There are many ways to reduce these risks, but due to the high incidence of bone breaks in the aging population new treatment and prevention methods are still needed. A possible treatment method is to reintroduce bone forming components into the bone directly through an electrospun resorbable implantable device. This device could help activate the bone formatting cells to create new strong bones and help reduce the risk of an osteoporotic fracture.

CHAPTER 2
LITERATURE REVIEW

2.1. Introduction to Electrospinning

2.1.1. Electrospinning Overview

Nanometer sized materials have become increasingly popular in recent years in the field of tissue engineering because they are similar in scale to many biological agents such as proteins, viruses, and bacteria. If these objects could be successfully integrated into a scaffold and implanted into the body, they could be used in many biomedical applications such as drug or protein delivery (Liu et al. 2011; Park et al. 2002; Wang and Spector 2009). The ideal immobilization scaffold should be on the nanoscale, and have the ability to facilitate the interaction of the biological agents of interest (Greiner wt al. 2006). There are various ways to make such nanofiber immobilization scaffolds that include drawing, template synthesis, phase separation, self-assembly, and electrospinning. Electrospinning is of particular interest because of its convenient processing and known repeatability (Ramakrishna et al. 2005). It can also be used with a wide range of polymers to develop a scaffold that is made up of a randomly oriented porous nanofiber network.

The formation of fibers by electrospinning was first patented by Anton Formhals in 1934 (Formhals 1934). The use of these fibers for biological applications was then introduced in 1977 by Graham Martin, where electrospun organic polymers were suggested as wound dressings (Martin 1977). Subsequently, in the 1990s it was demonstrated that a wide range of natural and synthetic polymers could be used in the electrospinning process. These materials are ideal because of their biocompatibility and

biodegradability (Greiner et al. 2006). Since then, electrospinning has been associated with the tissue engineering of three dimensional scaffolds. Tissue engineering is defined as creating or repairing damaged tissue or organs by fabrication of a three dimensional scaffold, which combines biological agents and biomaterials that can support cell proliferation (Lannutti et al. 2007).

The process of electrospinning utilizes an external electric field to apply a charge to a small drop of polymer solution that directly opposes the surface tension of the solution. Once the charges overcome the surface tension of the solution, a thin jet of electrically charged solution is created. The jet moves toward the grounded return plate as the solvent evaporates leaving a solid polymer nanofiber that is collected (Bai et al. 2007; Cui et al. 2007; Lannutti et al. 2007). A schematic of the electrospinning process is shown in Figure 2.1. The jet that is formed is known as a Taylor Cone, which occurs when the critical voltage applied to droplet of solution overcomes the surface tension of the solution, resulting in a thin jet that moves in a conical direction towards the return electrode (Matthews et al. 2002; Shin et al. 2001).

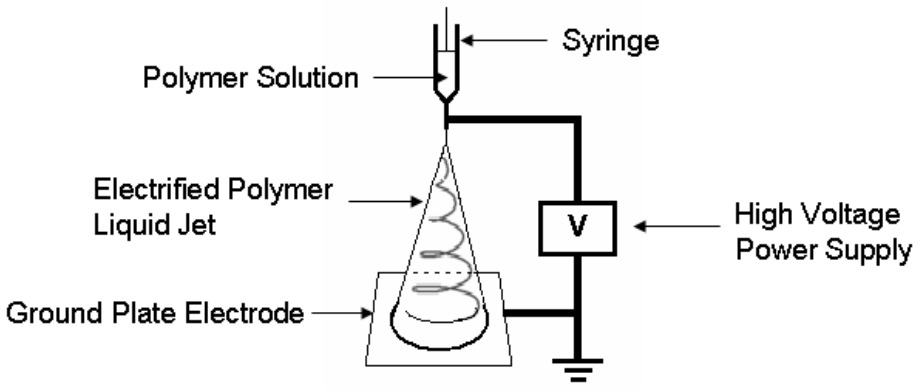

Figure 2.1: Electrospinning schematic

Electrospinning is popular due to its simplicity and versatility for the creation of a broad range of nanoscaffolds (Rafique et al. 2007). The morphology of the polymer mesh is beneficial because it can be made to mimic different types of extracellular matrix (ECM). The ECM is composed of many different proteins that are assembled into meshwork associated with the cells that produced them (Ramakrishna et al. 2005). The key components of ECM mimicking mesh is a porous structure that allows good cell proliferation, a large surface area for bioactive molecules to be seeded, and a degradation rate that pairs with the regeneration of the natural tissue type (He et al. 2005; Kim and Park 2006). In order to create the nanofiber mesh with these desired characteristics, there are many fabrication parameters that must be addressed.

2.1.2. Parameters to Control Fiber Formation

As mentioned in the previous subsection, electrospinning utilizes an external electrical supply applied to a polymer solution to make nanofiber meshes that can be used in the field of tissue engineering (Hsu et al. 2010; Jose et al. 2009). A charge is applied to the tip of a needle containing the polymer solution where, once the surface tension of the solution is overcome by the buildup of charge, a nanofiber is formed that travels to the ground plate as the solvent dissolves. The versatility of the nanofiber meshes comes from many of the parameters that can be adjusted to affect fiber formation, diameter, and alignment. These parameters fall into two distinct categories: solution parameters or apparatus parameters.

Solution parameters include the polymer, solvent, surface tension, and viscosity. The polymer in the solution is the most important factor in electrospinning because it defines the chemical makeup of the nanofiber and dictates potential tissue engineering applications based on the polymer that is utilized. Solvent composition is also important

depending on the polymer that is selected because it must effectively dissolve the polymers to create a homogeneous solution. Additionally, the solvent needs to evaporate quickly enough for the fiber to maintain its shape when it reaches the collector, but not so quickly that the fiber does not reach an appropriate diameter in the nanometer range (Ramakrishna et al. 2005). The two solution parameters of importance that can be adjusted based on the polymers used and solvents chosen are surface tension and viscosity, which determine the amount of stretching of the solution (Ramakrishna et al. 2005).

Surface tension is the intermolecular attraction of solution molecules that allows it to resist an external force. It is this force that gives a drop of water on a flat surface its identifiable droplet shape. It is also a function of the components that make up the solution. In electrospinning, surface tension is important because the charge on the polymer solution needs to be large enough to overcome the surface tension of the solution so it forms the necessary jet (Ramakrishna et al. 2005). If the surface tension is too high, the drop will form at the needle tip and remain there until the size of the drop and the effects of gravity force it to fall. Surface tension is also closely related to viscosity.

Viscosity describes a solution's resistance to flow. Viscous solutions are resistant to flow and non-viscous solution flow freely. Viscosity is important because highly viscous solutions to prevent the jet from forming, while non-viscous solutions allow the fluid to flow freely from the needle (Ramakrishna et al. 2005). In terms of nanofiber morphology, as the viscosity or surface tension is decreased, the fiber diameter is decreased and vice versa (Lannutti et al. 2007). This means that fluid thickness could help control or modulate fiber diameter by changing polymer concentrations because viscosity and surface tension increase as polymer concentration increases (Lannutti et

al. 2007; Spasova et al. 2007). Viscosity is also affected by molecular weight, where higher molecular weight polymers have higher viscosities. Higher molecular weight polymers also decrease the risk of beading within the fiber, and a have a higher degree of chain entanglement which improves the mesh morphology (Ramakrishna et al. 2005).

Apparatus parameters include voltage, ground plate to needle distance, flow rate, needle gauge, ground plate material, and humidity. Apparatus parameters affect the morphology of the nanofiber. These parameters can be controlled by the user once the desired solution is created. They can also be adjusted in real-time as a mesh is being formed to ensure consistent fiber formation. Ramakrishna et al. (2005) describes voltage as being the most crucial apparatus parameter because it initiates the electrospinning process by inducing the necessary charges on the solution. The voltage needs to be sufficient to overcome the viscosity and the surface tension of the polymer solution to maintain a jet from the needle tip containing the solution. It can be associated with the force of gravity, because it is the force pulling the liquid down towards the collector plate. A larger applied voltage increases the net charge experienced by the jet, which increases its electrostatic pull and creates smaller fiber diameters (Cui et al. 2007). A larger voltage also pulls the solution from the needle at a faster rate which may be beneficial with more viscous solutions (Ramakrishna et al. 2005). The required voltage to initiate electrospinning is also impacted by the electrode separation distance.

Ground plate to needle distance (electrode distance) is measured from the needle tip to the ground plate surface. If the working distance is too long, the electrical charge at the needle tip will not feel the pulling force from the ground plate (Kim et al. 2008). This will cause the solution to bead at the needle tip and drip onto the ground plate without the solvent evaporating or nanofibers forming. To overcome this problem, the separation distance should be decreased slightly until fibers begin to form, without

dripping, at the voltage that has been selected. If the plate separation is too small, however the solvent does not have time to evaporate. To overcome this problem, the separation distance should be increased and the voltage should be reduced accordingly. Large separation distances could also allow more time for the solvent to dissolve so the nanofibers could have a smaller diameter. All of these factors should be considered when selecting the electrode distance and corresponding voltage to create a uniform nanofiber mesh.

Flow rate is the amount of solution that is readily available for electrospinning at the needle tip. For a given voltage there is a corresponding flow rate that generates the most stable Taylor cone and nanofiber formation (Ramakrishna et al. 2005). The flow rate should be adjusted so there is a consistent drop at the end of the needle tip to facilitate the electrospinning process. If it is too slow, the solution will not spin at a constant rate, and if the rate is too fast, then the solution will drip out without spinning properly. Additionally, if it is too slow, the solvent may evaporate at the needle tip, causing a clog, and preventing the electrospinning process. Flow rate is also correlated to solution concentration and viscosity. A more viscous and concentrated solution will take more time to spin once at the needle tip, so the flow rate should be reduced (Garg and Bowlin 2011).

Needle gauge affects the size of the solution drop that is exposed to the external forces that initiate electrospinning. Needle gauge is opposite of needle diameter, so larger diameter needles represent a smaller gauge needle. Large gauge needles expose smaller droplets of solution that have larger surface tensions, and small gauge needles expose larger droplets of solution with smaller surface tension. With larger gauge needles, the surface tension of the polymer solution is larger, so at a constant voltage more force is required to start electrospinning (Ramakrishna et al. 2005). This means

that solutions with an inherently high surface tension may not spin with large needle gauges because the applied voltage cannot overcome the surface tension of the solution. Large gauge needles could also cause clogging of the needle tip if the solution is viscous and the solvent evaporates quickly. Small gauge needles could also be dangerous because the solution could flow more easily, not allowing the electrospinning process to initiate (Garg and Bowlin 2011). For these reasons, needle gauge should be altered to fit the solution as needed.

The choice of ground plate material is important because it must create an electric field between the supply and the collector for the electrospinning process to be initiated. The main constraint is that it needs to be a metal, or the nanofibers will not deposit correctly (Garg and Bowlin 2011). For most electrospinning procedures, any metal is sufficient as the ground collector plate. The material itself has very little effect on fiber morphology or the electrospinning process. The ground plate size is also important, because the plate needs to be large enough to collect all of the nanofibers. The size of the mesh is largely determined by the Taylor cone and the electrode distance. This is seen because the larger the electrode separations distance, the larger the Taylor cone, and the larger the mesh.

Humidity can also affect the electrospinning process by altering the rate of solvent evaporation. In a very low humidity environment volatile solutions may evaporate too quickly to electrospin and the needle tip may become clogged by the solidified polymer. In very humid environments water could condense on the nanofiber mesh, altering the morphology (Garg and Bowlin 2011). These effects may be difficult to control in some laboratories, but they should be noted as effecting nanofiber formation if there is a large variation in fiber morphology if all other parameters remain unchanged.

The solution and apparatus parameters are vital to the electrospinning process. The process of electrospinning appears simply; but, complexity in the actual fabrication process comes from the numerous ways these parameters can be altered to create a desired tissue engineered material. The first step is selecting the polymers and proper solvents that can dissolve the polymers and create a solution that can be electrospun. To be utilized in tissue engineering applications, a polymer should be selected based on the biological interactions it will have once implanted so it can properly integrate into the body. After the solution is created, the other parameters need to be carefully balanced to generate a nanofiber mesh with the required porosity and uniform fiber morphology.

2.2. Collagen and Hyaluronic Acid Electrospinning

Many diseases can lead to untreatable damage to the body. Utilizing engineered tissue equivalents could help reduce the side effects of such diseases. Challenges in this research field are creating biomaterials that have suitable biocompatibility, degradation properties, and mechanical properties for their desired application (Homenick et al. 2010). Electrospinning has been utilized to create nanofiber mesh materials that could aid in the treatment or prevention of some of these diseases. To make the electrospinning solution, the desired application needs to be studied to determine what polymer combination will provide the best results. In the disease osteoporosis, bone strength is reduced, which increases the risk of a bone fracture. If a tissue engineered material could be created to increase bone strength, the risk of bone fracture could be reduced and the effects of osteoporosis could be diminished.

Many synthetic polymers have been used in electrospinning applications. These include polylactic acid (PLA), polyglycolide (PGA), poly(lacitide-co-glycolide) (PLGA), or polycaprolactone (PCL). These polymers are often good electrospinning candidates

because of their biocompatibility and known degradation rates (Kim et al. 2008; Vassalli 2008). Natural polymers such as collagen, silk, fibroin, chitosan, and hyaluronic acid could also be used in electrospinning to create a desired scaffold (Kim et al. 2008; Matthews et al. 2002). Of particular interest are collagen and hyaluronic acid, due to how their unique biological properties function in the ECM.

Collagen is also a good candidate to be used in electrospinning for several reasons. First, collagen is the most abundant protein in the body where it acts as a structural building block of the ECM found in most native tissues (Hsu et al. 2010; Tan et al. 2010). Second, collagen possesses natural binding sites for the adhesion of osteoblasts, which aid in bone formation (Jose et al. 2009). Third, it has known chemical, mechanical, and biocompatible properties. Fourth, there are many processing methods that can be used to isolate collagen in large quantities (Homenick et al. 2010). Lastly, it has the ability to increase cell adhesion and the differentiation of many cells (Hsu et al. 2010). Unfortunately, collagen alone does not have the mechanical and structural support to perform well after implantation. This has led to research in crosslinking it with other, more robust, materials such as hyaluronic acid (Homenick et al. 2010; Tan et al. 2010).

Hyaluronic acid (HA) can be found in the ECM of connective tissues and has unique viscoelastic properties as well as good biocompatibility and biodegrability that make it a good candidate for tissue engineering (Hsu et al. 2010; Ji et al. 2006). Electrospinning using HA can be difficult because of its high viscosity and surface tension, even in low concentrations, and its hydrophilic nature that may not be favorable for some applications (Hsu et al. 2010). Because of these complications, electrospinning nanofibers containing both collagen and HA has not been seen in research until recently.

Individually, these two materials are not good candidates for electrospinning, but combined they could combine unique properties to be successful in tissue engineering. HA can modulate several cell behaviors, but does not readily promote cell adhesions because it is hydrophilic and it has low mechanical strength. Collagen promotes cell adhesion and can promote good tensile strength (Kim et al. 2008). After the polymeric components are selected, appropriate solvents must be selected to facilitate the electrospinning process.

2.3. Gold Nanoparticles

Gold nanoparticles (AuNPs) have attracted recent interest because they are the most stable metal particle. They also have electronic, magnetic, and optical properties and can be used as catalysts in biology (Bai et al. 2007). Based on these properties AuNPs could be used in many biomedical applications related to biosensors, drug delivery, imaging, and tissue engineering (Gu et al. 2009). When combined with an electrospun polymer nanofiber mesh AuNPs could enhance cell proliferation and antimicrobial properties. AuNPs can be crosslinked to collagen with the aid of a non-toxic, zero length crosslinker, 1-ethyl-3-(3-dimethylaminopropyl) carbodiimide hydrochloride (EDC). The EDC is zero length which means it does not become part of the scaffold, it only acts to activate the functional groups on the collagen to form the amide bond with the gold. Cell viability studies can then be performed to see if the AuNPs promote cell growth and biocompatibility, and animal studies can be performed to determine if there is an increased cell proliferation and tissue in-growth. Some *in-vivo* rat studies have also been performed with collagen based ECM materials crosslinked with AuNPs that have shown good biocompatibility and an optimization of properties associated with cellularization and ECM formation (Deeken et al. 2011).

CHAPTER 3
INTRODUCTION TO RESEARCH

3.1. Significance of Research

The motivation of this research is the worldwide burden osteoporosis places on society. There are several commercially available therapies to help reduce the effects of osteoporosis. These include vitamin supplements, hormone therapy, and pharmaceuticals, all of which are designed to promote new bone growth or limit bone resorption by targeting the bone formation cells. The problem with many of these therapies is the need for continual use to be effective, or their limited effectiveness after bone loss has already began. Additionally, there are many risk factors affecting the onset of osteoporosis that cannot be altered by these treatments. By innovating an implantable mesh that could increase the bone material itself, instead of the cells that promote its formation, the treatment of osteoporosis could be transformed.

Collagen is the most abundant protein in the body and is the main component of bones and the ECM of many tissues. Additionally, hyaluronic acid is a main component of the ECM of connective tissue. It may be possible to promote new bone growth by reintroducing these two components directly to the bone through a tissue engineered biomaterial. Such a material could be created using a nanofiber mesh created trough electrospinning. Electrospinning utilizes a high voltage supply to draw a polymer solution into nanofibers that can be collected to create a porous mesh material. By selecting natural polymers such as collagen and HA, the biocompatible meshes could integrate into the human body through cellular in-growth and promote the growth of new bone components that is stronger, thus reducing the effects of osteoporosis.

3.2. Research Objective

The objective of this research was to electrospin a collagen and hyaluronic acid nanofiber mesh, characterize the material, and determine biocompatibility. The research progressed in three separate stages. Phase one (Chapter 4) was to develop the nanofiber mesh and determine the appropriate electrospinning parameters. Phase two (Chapter 5) was to conjugate gold nanoparticles (AuNPs) onto the mesh. The final phase (Chapter 6) was to conduct a cell assay to determine cellular response of the nanofiber meshes.

Phase one was the most involved stage because it involved setting up the electrospinning apparatus and altering the different parameters to get consistent fiber formation. Research performed by Vassalli et al. (2008) created the electrospinning platform and all of the necessary components. The main components can be seen in Figure 3.1. They include 1) a Plexiglas box, 2) a high voltage power supply, 3) a syringe pump, 4) a ground plate collector, 5) dispensing needle, and 6) a needle height adjusting knob. The adjustable parameters included voltage, needle to ground plate distance, flow rate, and solution concentration. During this phase, all of these parameters were altered in order to get the most consistent fiber formation possible. In particular, solution concentration was studied to get a solution that would have the longest working time, without becoming too viscous to spin properly. After the meshes were created, Fourier transform infrared (FT-IR) was used to characterize the surface composition.

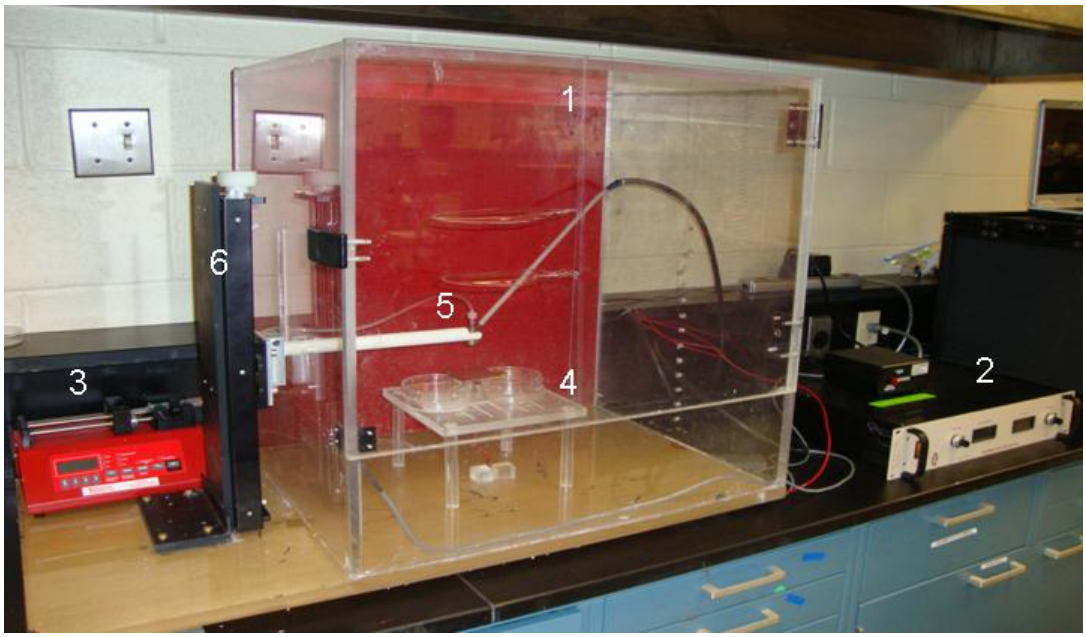

Figure 3.1: Electrospinning apparatus depicting the six main device components

Phase two consisted of conjugating AuNPs to the mesh surface. The AuNPs are in a water based solution, and an unfortunate property of the collagen/HA mesh is that it dissolves in water. To overcome this problem an ethanol and carbodiimide (EDC) crosslinking procedure was performed on the nanofiber meshes. This process modifies the protein side groups so they form bonds between themselves and no longer dissolve in the water based solutions. This step was also important because phase three involves a water based cell assay. After the crosslinking, AuNPs were conjugated to the mesh surface. To ensure conjugation scanning electron microscope (SEM) and energy dispersive spectroscopy (EDC) were used to take images of the nanofibers and pinpoint the gold.

Phase three consisted of a water soluble tetrazolium (WST-1) assay to test cell viability and biocompatibility. In this assay the meshes were exposed to a common cell line to determine the effects of the AuNPs on the meshes. In order to be biocompatible, the meshes need to support the growth of cells successfully and not exhibit any toxic effects. If successful, these experiments will create a biocompatible nanofiber mesh scaffold that is functionalized with AuNPs that allows cellular in growth and promotes the growth of new strong bone in osteoporosis patients.

CHAPTER 4
ELECTROSPINNING COLLAGEN AND HYALURONIC ACID

4.1. Introduction

New bone formation in osteoporosis patients could be possible by electrospinning a collagen and hyaluronic acid nanofiber mesh. The goal of this natural scaffold is to seamlessly integrate into weak bone to introduce new collagen and hyaluronic acid into the bone and promote bone formation by activating bone forming cells. Collagen is a major structural protein of the ECM and is the main component of bone (Wang and Spector 2009). Hyaluronic acid can be found in some connective tissue and can be paired with collagen to make a biocompatible nanofiber mesh material when processed correctly (Park et al. 2002).

In order to promote and support the regeneration of bone tissue, the collagen and hyaluronic nanofiber mesh must have uniform fiber diameter and porosity (Wang and Spector 2009). This will require optimization of both solution and apparatus parameters to create a reproducible experimental setup that can create a consistent and uniform nanofiber mesh. The following experimentation was executed to learn about the effects of different parameters on the electrospinning process. Fourier transform infrared (FT-IR) spectroscopy and scanning electron microscopy (SEM) were both performed to characterize the material and visualize the fiber deposition and diameter. Based on the testing, the best solution concentration was determined and the optimal apparatus parameters were selected and justified.

4.2. Electrospinning Apparatus

The electrospinning apparatus was previously designed and tested by Vassalli (2008). The main components of the device are a Plexiglas box, a high voltage power supply, syringe pump, ground plate collector, dispensing needle, and needle height adjusting knob. The apparatus can then be manipulated to electrospin any desired polymer solution with proper viscosity and surface tension by adjusting the apparatus parameters.

The main component of the electrospinning apparatus is the Plexiglas box seen in Figure 4.1. It is designed to house the ground plate collector and dispensing needle. It also provides safety by separating the highly charged electrospinning area from outside interference. The design also minimizes air flow irregularities that could disrupt nanofiber formation or disrupt the electric field. There is a safety latch on the box that is connected to a switch box that can be seen in the upper portion of Figure 4.2. The switch does not allow the voltage supply to be turned on unless it is in the locked position. It is then designed to automatically turn off the voltage supply if the box is opened while the power is on. The high voltage power supply can be seen in the lower portion of Figure 4.2. It is a Glassman High Voltage INC (High Bridge, NJ) EL30P01.5 and has a maximum voltage output of 30 kV and 1.5 mA current. The high voltage power supply is attached to the needle tip and to the ground collector plate to complete the circuit.

The syringe pump can be seen in Figure 4.3. It is a Braintree Scientific (Braintree, MA) BS-8000 series syringe pump that can be adjusted to flow rates between 0 and 99 ml/hr. The syringe holding the polymer solution is inserted into the pump system. The syringe is attached to the dispensing needle through Cole-Parmer 1/16” diameter TYGON lab tubing (Vernon Hills, IL) and Cole-Parmer male and female 1/16”

hose barbs. The pump is located outside of the safety box and the TYGON tubing carries the solution into the isolated box to the needle.

The ground plate collector and dispensing needle can be seen in Figure 4.4. They are both located inside of the Plexiglas box so they can be separated from the outside environment. The dispensing needle holder is attached to a ceramic rod that attaches to the needle height adjusting knob seen in Figure 4.1. It is also attached to an electrode from the voltage power supply. There is a Plexiglas base that lifts the ground collecting plate so the proper separation distance can be achieved. The ground pate is attached to the other electrode from the voltage supply. The ground plate electrode is attached to a 1x3 inch copper plate, but can be altered based on solution needs as long as it remains conductive. The Plexiglas base holding the collecting plate can be removed for solutions that require larger separation distances. The adjusting knob can also be used to raise and lower the needle height as needed.

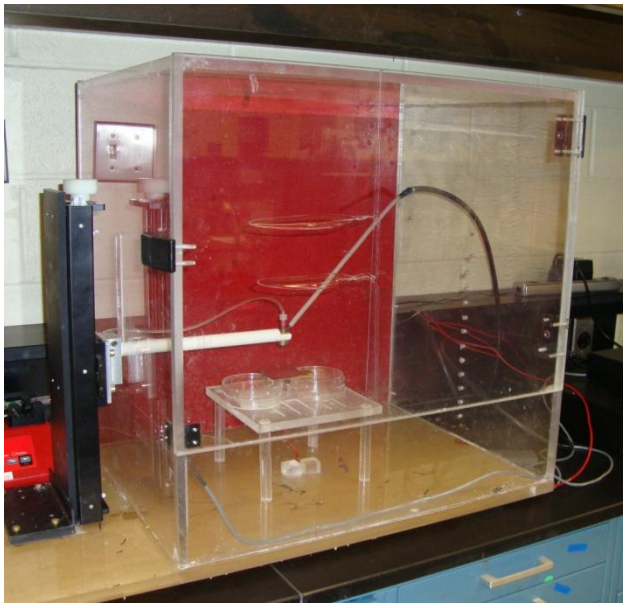

Figure 4.1: Plexiglas box and needle height adjusting knob

Figure 4.2: High voltage power supply directed and switch box for safety to ensure the Plexiglas box is closed.

Figure 4.3: Syringe pump that controls the flow rate of the polymer solution

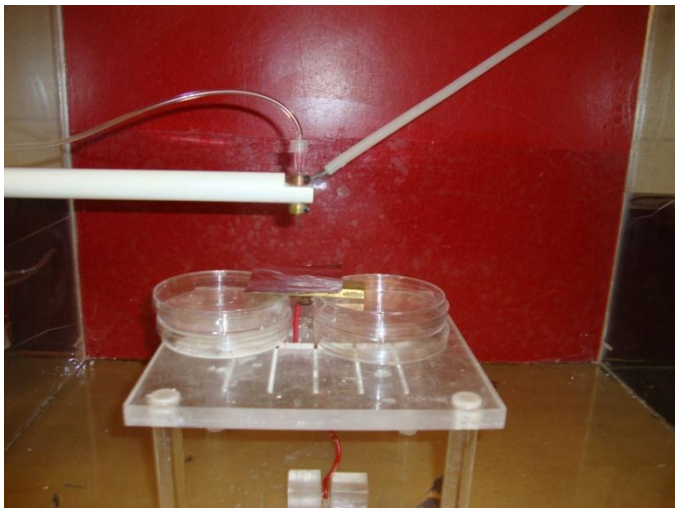

Figure 4.4: Ground plate collector where the nanofiber mesh is deposited and dispensing needle that holds the polymer solution

4.3. Materials and Methods

4.3.1. Electrospinning Solution Parameters

The solution parameters that determine if a solution can be electrospun are its viscosity and surface tension. These are dependent on the polymer that is selected and its concentration in the solvent. Collagen and hyaluronic acid were the pre-selected polymers for this experiment. The variables that could be altered were the polymer concentrations, the solvents, and the solvent ratios. The collagen used for testing was Calf Skin Collagen from Sigma Aldrich (St. Louis, MO). The Hyaluronic acid used for testing was Sodium Hyaluronate (m.w. = 601k-850k) from Lifecore Biomedical (Chaska, MN). The solvents that were used for experimentation were sodium hydroxide (NaOH) and dimethylformamide (DMF). Solution parameters were based on an article by Kim et al (2008). His experiment used 10% weight to volume HA/collagen in 95/5 and 80/20 weight ratios dissolved in a 4/1 volume to volume ratio of NaOH/DMF (Kim et al. 2008). A summary of the solution parameters can be seen in Table 4.1. These parameters were used for the initial electrospinning procedures and altered to obtain a solution that could be spun easily and obtain a consistent nanofiber mesh scaffold.

Table 4.1: Initial electrospinning solution parameters Kim et al. (2008)

	NaOH/DMF (vol/vol)	Solids (% weight)		Solids to liquids (% weight/vol)
		Hyaluronic Acid	Collagen	
Kim et al. (2008)	4/1	95%	5%	10%
	4/1	80%	20%	10%

4.3.2. Electrospinning Apparatus Parameters

Once the different solution parameters are selected, fiber formation is dependent on the proper selection of the apparatus parameters. Parameters such as voltage, plate separation distance, flow rate, and needle gauge all have drastic effects on fiber formation. They are all interdependent and must be optimized to generate the most uniform fiber mesh. Like the polymer solution, the article by Kim et al. (2008) helped determine the initial apparatus settings. In initial testing the voltage was set to 16 kV, needle gauge was 23, a plate separation of between 3-5 cm (it did not specify the exact distance that was used), and flow was 10 µL/min (Kim et al. 2008). A summary of these parameters can be seen in Table 4.2.These were then altered as needed to generate the most uniform scaffold. Aluminum foil was selected as the ground plate collector, because it is conductive, inexpensive, and pliable. Pliability was important because it would allow the scaffolds to be easily removed from the metal surface by peeling the foil away from the scaffold. Other thicker metal plates could also be used, but it would have been more difficult to remove the scaffolds and could have resulted in mesh defects or deformation.

Table 4.2: Initial electrospinning apparatus parameters Kim et al. (2008)

Parameter	Settings
Voltage	16 kV
Needle Gauge	23
Plate Separation	3-5 cm
Flow Rate	10 µL/min

4.3.3. Challenges in Electrospinning Process

The biggest challenge in the electrospinning process was creating a viable solution that could be electrospun. The molecular weight of the hyaluronic acid is 601k-850k which is very high. This makes the solution very viscous and difficult to spin at high concentrations.

High molecular weight polymers have longer monomer chains and thus an increased amount of chain entanglement which makes it more viscous (Ramakrishna et al. 2005). The problem is compounded when the monomer needs to be dissolved in a solvent solution that evaporates quickly. For the HA, this resulted in a very short working time once the HA was added to the solvent solution: once the HA was dissolved in the solvent, it could be electrospun for about one hour before it became too viscous to spin properly.

In addition, the collagen did not dissolve readily in the solvent solution. If the collagen was added when the HA was added the collagen did not dissolve before the HA became too viscous to spin. To overcome this problem, the collagen was added to the NaOH at least 12 hours before electrospinning. This would allow it to dissolve properly. Then, the DMF and HA were added and the solution could be electrospun for about one hour until it was too viscous to flow freely. When the solution would begin collecting at the needle tip and drip onto the scaffold forming on the ground electrode, then the electrospinning was completed.

There were additional problems associated with humidity in the laboratory. The electrospinning is influenced by the environment in the room. On dry days it was very difficult to electrospin because the solvent dissolved very quickly. This shortened the working time of the solution from one hour to around 30 minutes. On these days there was also a less consistent nanofiber deposition. On very humid days, the solvent did not

dissolve as readily, and it would cause the solution to drip onto the ground electrode, making electrospinning difficult. The most desirable days had a humidity of 20-40% in the laboratory when the solvent evaporated at a consistent rate which allowed for very uniform nanofiber deposition. In order to prevent nanofiber alterations due to humidity effects, the electrospinning set-up should have a humidity controlled environment.

4.3.4. Surface Analysis of Meshes Using FT-IR

Fourier transform infrared (FT-IR) spectroscopy is a detection method that measures the wavelength of bonds on the surface of a material through absorption. Spectra were collected by a Nicolet 6700 FT-IR spectrometer (Thermo Fisher Scientific, Waltham, MA). During the spectra collection different wavelengths of infrared light pass over the sample and it measures how much of the light is absorbed at each wavelength. Each wavelength corresponds to a particular chemical bond and absorption of light signifies a bond. Based on the peaks in the scan the different bonds in a material can be identified.

The FT-IR spectrum can be likened to a fingerprint; a material will present different peaks that represent the chemical makeup of the material. FT-IR spectroscopy can also be used to detect surface changes that are made during functionalization of a material. This type of characterization was utilized to confirm that the fabricated scaffolds was a collagen and hyaluronic acid blend as well as to determine what surface changes were made during each additional processing step.

4.3.5. Mesh Analysis Using SEM/EDS

After the HA/collagen nanofiber meshes were created a scanning electron microscope (SEM) was utilized to acquire detailed images of the nanofiber scaffolds. These images are valuable to demonstrate that a uniform nanofiber mesh is created. Based on the fiber deposition from the images, polymer concentration changes can be made to improve the fiber deposition. SEM images were taken using a Quanta^{TM} 600 scanning electron microscope with a field emission gun (FEG) system (FEI Company, Hillsboro, OR). Electron dispersive spectroscopy (EDS) was also performed to determine the composition of charged particles from SEM images. This elemental analysis was performed by a Thermo Scientific NORAN System Six microanalysis system (Thermo Fisher Scientific, Waltham, MA). The microscopy analysis was performed at the University of Missouri Electron Microscopy Core with assistance from Matthew Cozad.

The SEM can be adjusted in several ways to obtain the clearest image. Secondary electron detection is the most common setting and collects low energy electrons from the sample surface. This detection method is capable of high depth images where the electrons hit the surface and are ejected towards the collector. Backscatter electron imaging consists of high energy electrons that originate in the electron beam, hit the sample, and are reflected back. This detection method allows more surface detail, but has less image depth. Both methods were adjusted to view the samples at different magnifications so that the most detailed images were collected. From the images, measurements were made to determine the fiber diameter using the measurement software ImageJ. This data is useful to verify that nanofibers are being generated as well as to validate consistent of the mesh diameter.

4.3.6. Statistical Analysis

Statistical analysis was performed to compare the different data sets. All statistical analysis was performed using GraphPad Prism® software, version 4.0. This software was used to analyze the nanofiber diameter data from different SEM images. The data was plotted and the mean and standard deviations can all be graphically represented to better visualize the data that was obtained.

4.4. Results and Discussion

4.4.1. Solution and Apparatus Constraints

Initial testing was based on an article by Kim et al (2008). Solutions were made at 10% weight to volume HA/collagen in 95/5 and 80/20 weight ratios dissolved in a 4/1 volume to volume ratio of NaOH/DMF (Table 4.3). When the 80/20 weight ratios were made at a 10% wt/vol of solvents the collagen never fully dissolved into the solution. More solvent was added to create an 80/20 5% wt/vol solution. At this concentration the collagen fully dissolved and the solution would spin, but upon imaging the nanofibers did not have a uniform shape and had beads throughout.

At the 95/5 weight ratios the collagen would fully dissolve at a concentration of 10% wt/vol with the HA. However, this solution would not electrospin consistently, and had a very short working time because it was so viscous. The concentration was altered to 5% wt/vol of the polymers. This solution was much easier to work with and had a much longer working time. The optimal solution concentration that was selected was 7.5% wt/vol with a 95/5 HA/collagen ratio because it resulted in the most consistent nanofiber formation and uniform fiber mesh. Table 4.3 summarizes the suggested solution parameters, the experimental parameters and the final solution parameters that were selected. This selection was confirmed with the SEM images in a future section.

Table 4.3: Finalized electrospinning solution parameters

	NaOH/DMF (vol/vol)	Solids (% weight)		Solids to liquids (% weight/vol)
		Hyaluronic Acid	Collagen	
Kim et al. (2008)	4/1	95%	5%	10%
	4/1	80%	20%	10%
Experimental	4/1	95%	5%	10%
	4/1	95%	5%	5%
	4/1	80%	20%	10%
	4/1	80%	20%	5%
Optimal	**4/1**	**95%**	**5%**	**7.5%**

Like the polymer solution, the article by Kim et al. (2008) helped determine the initial apparatus settings. In initial testing the voltage was set to 16 kV, needle gauge was 23, a plate separation of 3-5 cm, and flow was 10 µL/min. Initial testing used these apparatus settings. During initial experimentation the solution would collect at the needle tip in very large drops and the electrospinning would not always initiate because of the high surface tension. This caused the solution to drip onto the ground plate instead of forming nanofibers. To overcome this problem, the needle was changed to 20 gauge, to increase the inner diameter and reduce the surface tension. Additional testing also showed that a plate separation distance of 5 cm generated the most uniform fiber mesh. At distances smaller than 5 cm the solvent would not evaporate as much and there would be uneven fiber deposition. The optimal apparatus parameters were set to a 20 gauge needle, 5 cm plate separation, 16 kV potential, 10 µL/min flow rate, and an aluminum foil ground plate collector. The final apparatus parameters are summarized in Table 4.4 and the finalized protocol can be seen in Appendix 1.

Table 4.4: Finalized electrospinning apparatus parameters

Parameter	Settings	
	Kim et al. (2008)	Optimal
Voltage	16 kV	16 kV
Needle Gauge	23	20
Plate Separation	3-5 cm	5 cm
Flow Rate	10 µL/min	10 µL/min

4.4.2. Surface Analysis of Mesh Using FT-IR

Knowing the molecular formula of a material is important to help determine what bonding will occur during functionalization. It can also help determine if the correct FT-IR spectra is obtained. The molecular formula for hyaluronic acid is $(C_{14}H_{21}NO_{11})_n$ and the molecular structure can be seen in Figure 4.5 (Chemblink 2011). The molecular formula for collagen is $C_4H_6N_2O_3R_2(C_7H_9N_2O_2R)_n$ and the molecular structure can be seen in Figure 4.6 (Chemblink 2011).

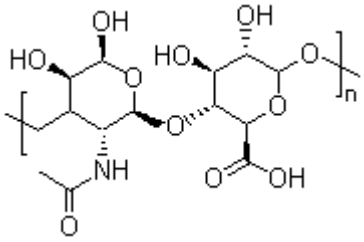

Figure 4.5: Molecular structure of hyaluronic acid (Chemblink 2011)

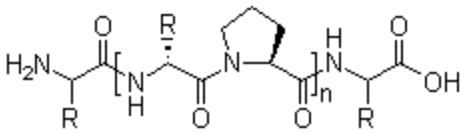

Figure 4.6: Molecular structure of collagen (Chemblink 2011)

The FT-IR spectra from hyaluronic acid and collagen can be seen in Figure 4.7. From the hyaluronic acid spectra there is a prominent amide N-H stretch from 3200-3600 cm^{-1}; there is an additional amide peak at 1595-1710 cm^{-1} that can be attributed to C=O stretching and N-H bending (Camacho et al. 2001; Chang and Tanaka 2002; Liu et al. 2006). There is also a C-H_2 bending peak from 1350-1480 cm^{-1} and C-O stretch of the proteoglycan sugar ring from 985-1140 cm^{-1} (Boskey and Camacho 2007; Camacho et al. 2001). From the collagen spectra there is a prominent N-H stretch from 3500-3600 cm^{-1} and a C-H_2 symmetrical stretching from 2850-2950 cm^{-1} (Camacho et al. 2001; Chang and Tanaka 2002; Muyonga et al.2004). There is also C=O stretching from 1720-1740 cm^{-1} and an amide peak attributed to C=O stretching and N-H bending from 1595-1710 cm^{-1} (Camacho et al. 2001; Chang and Tanaka 2002; Liu et al. 2006). Additional peaks from 1080-1360 cm^{-1} can be attributed to C-N stretching, N-H bending, and C-C stretching and a peak around 1200 cm^{-1} can be attributed to a C-O bond (Boskey and Camacho 2007; Camacho et al. 2001; Chang and Tanaka 2002). These spectra match the molecular structure which confirms their chemical makeup and bonding format.

Figure 4.8 displays the spectra of hyaluronic acid, collagen, and the 7.5% HA/collagen nanofiber mesh. It is obvious that the combination of the two polymers creates a unique spectrum that shares some prominent peaks from each of the individual components. The spectra in Figure 4.9 shows three different samples of the HA/collagen nanofiber meshes at 7.5% which was selected as the optimal polymer

concentration. Several different nanofiber mesh samples all had the same identifying peaks confirming that solutions created at different times still fabricated the same nanofiber mesh formulation. These samples were also taken over several months of electrospinning, which also shows consistency in the electrospinning process.

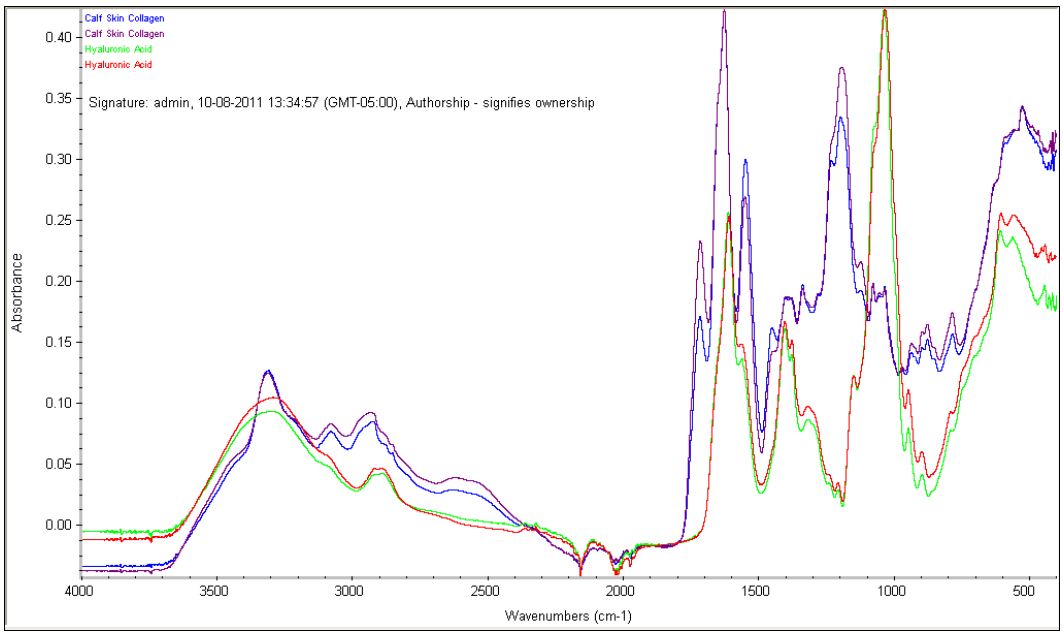

Figure 4.7: FT-IR scan of the raw materials; collagen (blue and purple) and hyaluronic acid (green and red)

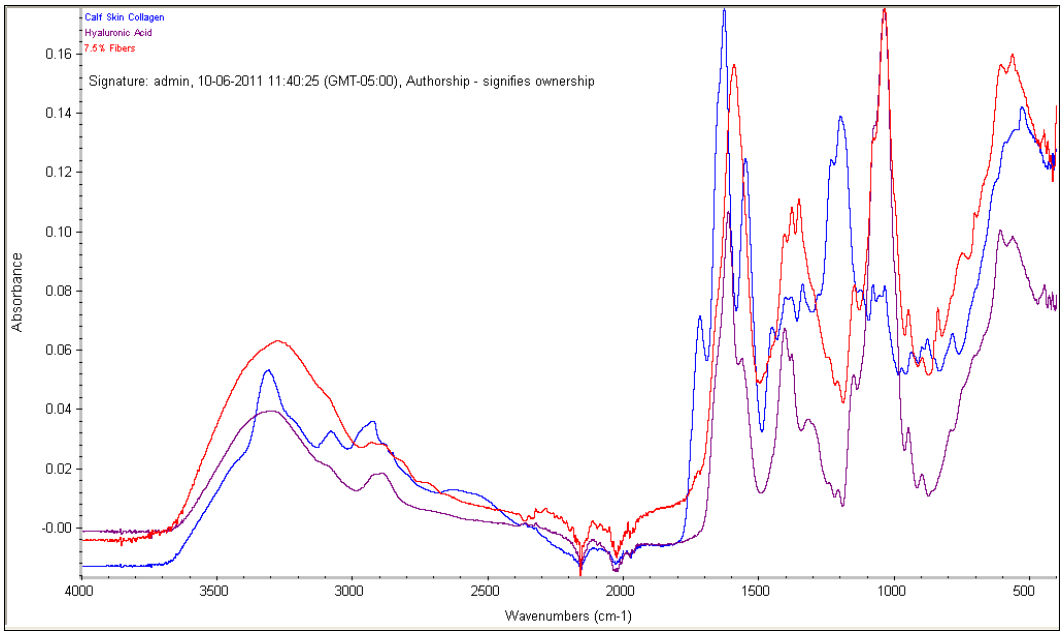

Figure 4.8: FT-IR scan hyaluronic acid (purple), collagen (blue), and 7.5% HA/collagen nanofiber mesh (red)

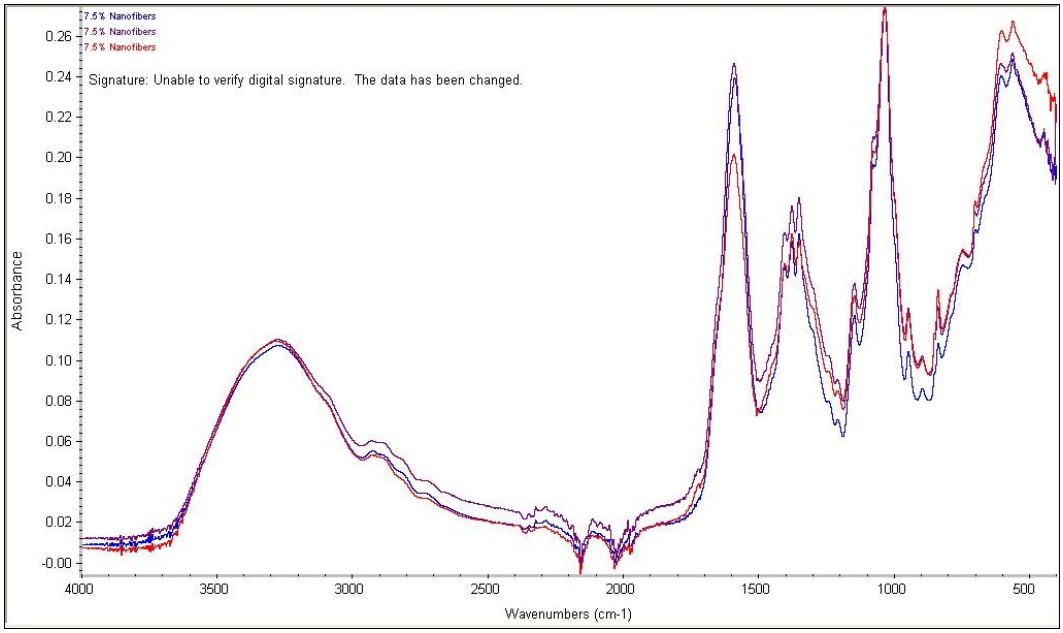

Figure 4.9: FT-IR scan of 7.5% HA/collagen nanofibers

4.4.3. Analysis of Nanofibers Using SEM/EDS

The SEM images of the nanofiber meshes shows a very detailed view of the nanofiber deposition. Figure 4.10 shows the 80/20 weight ratio nanofibers at 5% wt/vol. It is apparent that there is a random orientation of nanofibers. There also appears to be some beading because the topography appears roughen. Figure 4.11 shows the 95/5 weight ratio nanofibers at 5% wt/vol. This mesh is consistent with the 80/20 mesh, with a randomly oriented nanofiber network, but this image appears to have a less dense network, which could be due to a shorter electrospinning time resulting in a thinner nanofiber mesh. From this image the nanofibers appear to have even more beads that the 80/20 mesh. Beading is identifiably because the nanofibers are not smooth. Both of these images were taken using secondary electron detection mode.

Figure 4.12 shows the 95/5 nanofibers at 7.5%. This image was taken in backscatter mode, so it has less depth that the previous images, resulting in a smoother nanofiber deposition appearance. This image shows very smooth and consistent nanofiber formation. The 7.5% nanofibers are also larger in diameter than in the 5% wt/vol solution nanofibers (Table 4.5). There is also more inter-fiber webs in the 7.5% solution. Since all of the other processing parameters remained constant, the differences could be attributed to humidity changes. The more webbed nanofibers would suggest a more humid day where the solvent did not evaporate as much causing the nanofibers to adhere more on the return electrode.

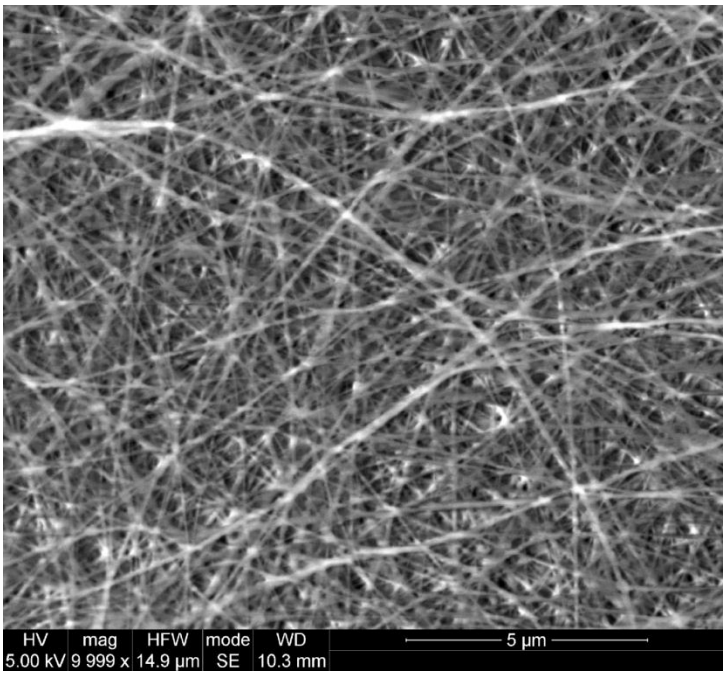

Figure 4.10: SEM image of HA/collagen 80/20 weight ratio, 5% wt/vol at 10,000X

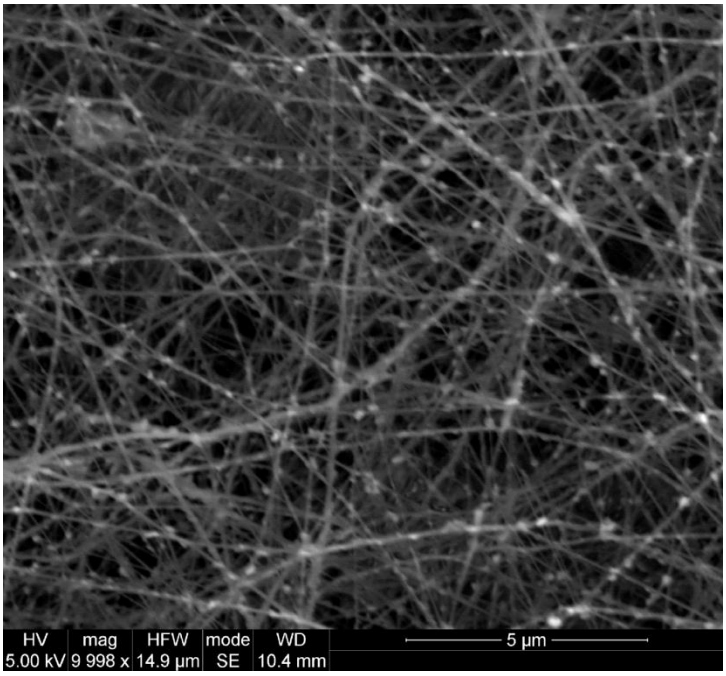

Figure 4.11: SEM image of HA/collagen 95/5 weight ratio, 5% wt/vol at 10,000X

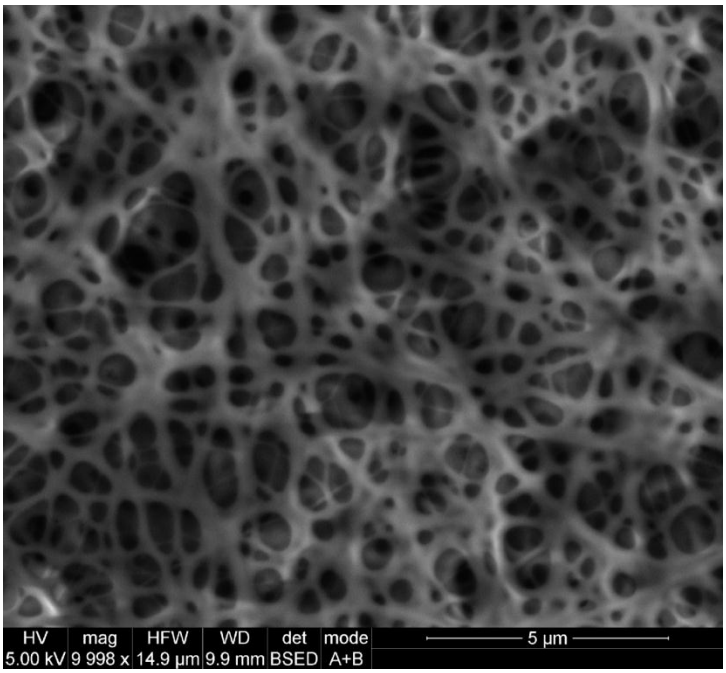

Figure 4.12: SEM image of HA/collagen 95/5 weight ratio, 7.5% wt/vol at 10,000X

4.4.4. Statistical Analysis Results

Data on the nanofiber diameter at three different solution concentrations was collected by two individuals using image processing software called ImageJ. In ImageJ, the three SEM images from Figure 4.10, Figure 4.11, and Figure 4.12 were used to measure the diameter of different fibers. Each researcher collected diameter data from 20 samples and then the data was combined and analyzed. This data can be seen in its entirety in Appendix 4 separated by the individual who collected the data. Table 4.5 shows a comparison of the average nanofiber diameters from the three different SEM images and the standard deviations of the data. This shows that the nanofibers at 5% concentrations were significantly smaller in size than the 7.5% concentration data. This data also confirms that nanometer sized fibers are being consistently fabricated. There is a larger standard deviation in the 7.5% data that can be attributed to the webbing that made that made measurement more challenging and inconsistent.

A graphical representation of the diameter data can be seen in Figure 4.13. The individual points are the different measured diameters at each concentration. The dotted red line represents the data mean and the red bracket represents the standard deviation. This confirms what the table confirms that the two 5% data sets have much smaller nanofibers and the 7.5% data has a wider range of larger nanofibers.

Table 4.5: Nanofiber diameter data collected from ImageJ

HA/collagen Concentration	5% 95/5	5% 80/20	7.5% 95/5
Average diameter (nm)	145.85	139.38	321.08
Standard Deviation	45.50	36.90	103.30

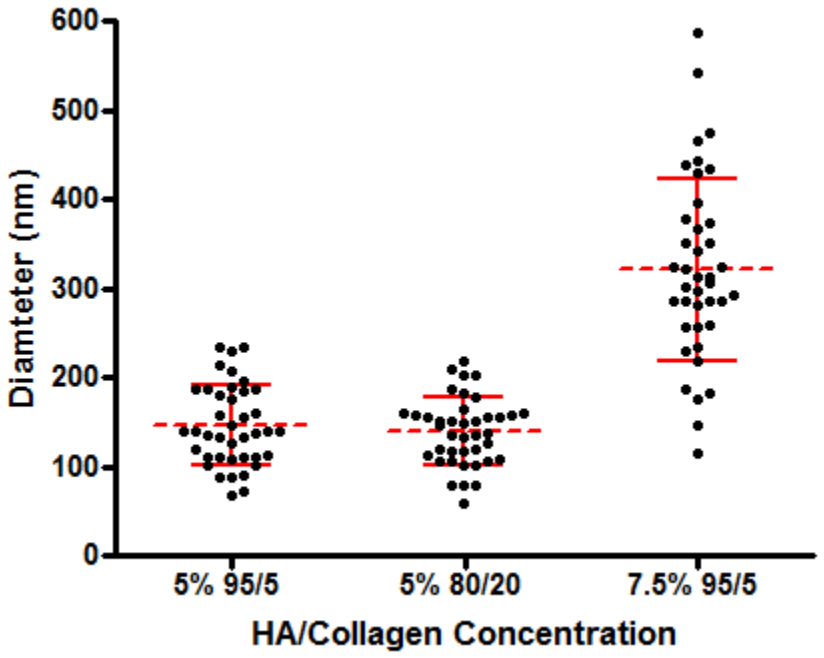

Figure 4.13: Nanofiber diameter data at different solution concentrations showing individual points (black dots), mean (dotted red line), and standard deviation (red bracket)

4.5. Conclusion

After experimentation with the different solution and apparatus parameters, an optimal procedure was successfully obtained to fabricate collagen and hyaluronic acid nanofiber meshes. The biggest challenges resulted from 1) the polymers dissolving into the solvents at different rates, 2) the working time of the solution, and 3) humidity effects. Resolutions were obtained to overcome these problems so the nanofiber meshes could be generated consistently.

From the images and data that was gathered it was determined that a 95/5 weight ratio of hyaluronic acid and collagen at 7.5% wt/vol dissolved in 4/1 (vol/vol) NaOH/DMF created an optimal polymer solution that produced smooth nanofibers meshes. The optimum apparatus parameters were a 20 gauge needle, 5 cm plate separation, 16 kV potential, 10 μL/min flow rate, and an aluminum foil ground plate collector. After electrospinning using this set-up a nanofiber mesh with consistent nanofiber diameters was developed. FT-IR spectra's displayed the distinct peaks of the mesh and also demonstrated that the mesh can be reproduced consistently. SEM images show the fiber morphology. Inconsistent fiber diameters were noted with the lower concentration solutions while consistent nanofiber deposition was achieved with the finalized solution. Diameter data shows that fibers are created in the nanometer range uniformly and consistently. These studies demonstrated that HA/collagen nanofibers can be consistently electrospun, but additional processing steps are required. The scaffolds need to be insoluble in aqueous solutions so the AuNPs can be attached and cell studies can be conducted.

CHAPTER 5
CROSSLINKING MESHES FOR BIOCOMPATIBILITY ANALYSIS

5.1. Introduction

The goal of tissue engineering is to create an extracellular matrix using biocompatible and biodegradable polymers (Wang and Spector 2009). This study utilized two naturally occurring polymers, collagen and hyaluronic acid, to fabricate nanofiber meshes that could be used in tissue engineering to help promote new bone growth. Initial experimentation found the optimal apparatus solution and apparatus parameters to generate a uniform nanofiber mesh. Since the collagen/HA meshes readily dissolve in aqueous solutions, it is necessary to crosslink them before any additional testing can be performed. Additionally, since it was desired to add gold nanoparticles (AuNPs) to the meshes, conjugation of the AuNPs was also required. First, a protocol was optimized to crosslink the meshes so they would not dissolve in aqueous solutions. Then, AuNPs were functionalized to the surface. Testing, using the FT-IR and the SEM, was then conducted to confirm the crosslinking steps and the presence of gold on the scaffolds.

5.2. Materials and Methods

5.2.1. Chemicals and Test Substances

A water soluble carbodiimide called 1-ethyl-3-(3-dimethylaminopropyl) carbodiimide hydrochloride (EDC) is commonly used as a crosslinking agent because it is a zero length crosslinker, which means the agent itself is not incorporated into the molecules (Barnes et al. 2007). EDC has a molecular formula of $C_8H_{17}N_3{\cdot}HClC_8H_{18}ClN_3$

and can be seen in Figure 5.1 (Chemblink 2011). It has been found to modify the side groups on proteins to allow bond formation between hydroxyl (-OH) and carboxyl (-COOH) groups of the HA making them insoluble in water (Park et al. 2002). The benefit of the EDC is that it does not become a part of the mesh, it just helps facilitate bonding within the mesh. Additionally, Sulfo NHS (*N*-hydroxysulfosuccinimide) was used in the conjugation procedure to aid in the attachment of gold nanoparticles. Sulfo-NHS has a molecular formula of $C_4H_4NNaO_6S$ and the molecular structure can be seen in Figure 5.2 (Chemblink 2011). To prevent the meshes from dissolving during the crosslinking process, ethanol was used as the solvent since the meshes are insoluble in ethanol. Phosphate buffered saline (PBS) was then used as a rinsing agent because it is non toxic to cells and can remove residual ethanol. After the crosslinking, an additional conjugation step was utilized to attach the AuNPs to the meshes.

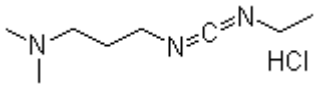

Figure 5.1: Molecular structure of 1-ethyl-3-(3-dimethylaminopropyl) carbodiimide hydrochloride (EDC) (Chemblink 2011)

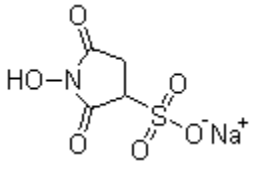

Figure 5.2: Molecular structure of *N*-hydroxysulfosuccinimide (Sulfo-NHS) (Chemblink 2011)

In order to crosslink the nanofiber meshes, they were first carefully removed from the aluminum foil, making sure they did not tear or crumple. Then the larger scaffolds were cut into 4.8 mm diameter circles and individually placed in a 48-well plate. The initial crosslinking procedure was adapted from Hsu et al. (2010). This procedure immersed the scaffolds in 5 mM EDC (Sigma Aldrich, St. Louis) in 95% ethanol for 24 hours, followed by a 24 hour 70% ethanol rinse and 0.1 M PBS wash to remove residual ethanol (Hsu et al. 2010).

5.2.2. Challenges in Mesh Solubility

After following the initial crosslinking procedure, the scaffolds still dissolved in the PBS rinse, which revealed that the initial EDC processing step was not crosslinking the mesh adequately. Additional research was conducted to find alternative crosslinking methods.

Park et al. (2002) crosslinked scaffolds using 1, 5, 10, and 50 mM EDC in 95% ethanol for 24 hours followed by a 5 minute rinse in distilled water. After the study they concluded that the 50 mM EDC solution retained the structure best and had a greater resistance to biodegradation. Wang and Spector (2009) used EDC and NHS (*N*-hydroxysuccinimide) in a 5:2 molar ratio in 80% ethanol for four hours to ensure solution infiltration into the scaffolds. Additional testing showed that crosslinking period should be longer than 2 hours and that they had better results with 80% ethanol than 95% ethanol. Jose et al. (2009) followed crosslinking both 5 mM and 50 mM EDC in 95% ethanol for 18 hours followed by a 1 M PBS rinse for 2 hours. Barnes et al. (2007) crosslinked using 20 mM EDC and 200 mM EDC for 18 hours then rinsed in 1 M PBS.

A optimization experiment was performed to determine what EDC concentration would crosslink the collagen/ hyaluronic acid scaffolds most effectively. All of the testing

was conducted using electrospun scaffolds from the optimized electrospinning protocol using 95/5 weight ratio of hyaluronic acid and collagen in a 7.5% wt/vol NaOH/DMF solution. Table 5.1 shows the three different variables that were assessed. They were: EDC concentration, ethanol concentration, and time.

Table 5.1: Crosslinking optimization experiment variables

	EDC Concentration (mM)	Ethanol Concentration (%)	Time (hr.)
Experimental	20	95	1, 2, 4, and 22
		80	1, 2, 4, and 22
	50	95	1, 2, 4, and 22
		80	1, 2, 4, and 22
	70	95	1, 2, 4, and 22
		80	1, 2, 4, and 22
Optimal	**50**	**95**	**22**

For this experiment meshes were cut into 4.8 mm diameter circles and placed in individual wells of a 24-well plate. There were two samples for each condition with a total of 48 samples. Next, 0.75mL of the corresponding EDC solution was added to each well for the allotted time. After the correct time the EDC solution was pipetted off and 0.75 mL of 1X PBS was added to test if the meshes dissolved.

In all of the 80% ethanol trials, the meshes shrank significantly when the EDC solution was added. They did not fully dissolve, but the diameter decreased significantly. All of the 95% ethanol meshes appeared stable and retained their size and shape in the EDC solution. After one hour, all 20 mM EDC meshes dissolved in the PBS rinse. Of the 50 mM EDC meshes, one 95% ethanol mesh dissolved and the 80% ethanol meshes re-

expanded to their original size and did not dissolve. During rinsing, all of the 70 mM EDC meshes appeared stable and retained their size and the 80% ethanol meshes re-expended to their original size. After two hours, the 20 mM EDC 95% ethanol meshes transitioned from the translucent white color to completely translucent so they were hard to identify in the well plate and they did not have a consistent shape. The 80% meshes regained their shape and size during rinsing. All other meshes in this time frame remained insoluble and did not dissolve in the PBS rinse. After 4 hours, all of the meshes survived the PBS rinse, but the 80% ethanol meshes did not completely regain their original size. After 22 hours, all of the meshes survived the PBS rinse. The 95% 50 mM EDC and the 95% 70 mM EDC were the easiest to identify in the well place and had the best color which was mostly translucent with hint of white so they could be identified in the well.

From this experimentation, it was determined that the optimal concentration and time would be 50 mM EDC in 95% ethanol for 22 hours. The 95% ethanol was selected because all of the 80% ethanol samples changed shape drastically when the initial solution was added, which is not ideal. Since the meshes are delicate it was also determined that using the lowest possible EDC concentration would be preferred, which was the 50 mM trial, even though the 70 mM samples were also successfully crosslinked.

5.2.3. Gold Nanoparticle Conjugation

After the crosslinking procedure was successfully optimized the AuNP conjugation was performed using chemical crosslinking. First, the meshes underwent the optimized crosslinking procedure of being placed in 50 mM EDC 95% ethanol solution for 22 hours. The AuNP conjugation was adapted from the Dr. Grant's biomaterials lab

(Cozad et al. 2008). For each mesh sample a solution of 4 mg EDC, 5.3 mg Sulfo-NHS (Sigma Aldrich, St. Louis, MO) and 0.25 mL distilled water was added to the well. After a few minutes, to allow the solution to penetrate the mesh, 0.25 mL of 100 nm AuNPs (Ted Pella, Redding, CA) was added. After one hour, the solution was pipetted off and 70% ethanol was added until further testing was performed.

5.3. Results and Discussion

5.3.1. Surface Analysis of Meshes Using FT-IR

FT-IR analysis was performed after each step in the crosslinking and conjugation process to assess the alteration of surface functional groups during the different processing steps. Figure 5.3 shows three scans of the 7.5% scaffolds after the crosslinking procedure. Figure 5.4 shows three scans of the 7.5% scaffolds after AuNP conjugation. Both shows consistency in the spectra with different samples confirming that crosslinking and conjugation results in consistent surface functionalization.

Figure 5.5 shows spectra of the 7.5% scaffolds before crosslinking, after crosslinking, and after AuNP conjugation. All of the spectra show very similar peaks. All of the samples are consistent at wavelengths greater than 2000 cm^{-1} where there is a very identifiable N-H bond seen in the peak 3000-3700 cm^{-1}. The most noticeable differences are a decrease in the peak from 1595-1710 cm^{-1} and a decrease in the peak around 1350 cm^{-1}. This could mean that some of the bond signatures are not as strong because the crosslinking and conjugation could damp and/or disrupt the bond formation. The many similarities are positive and show that there is no destruction of the chemical structure after the processing steps, which validated the protocols.

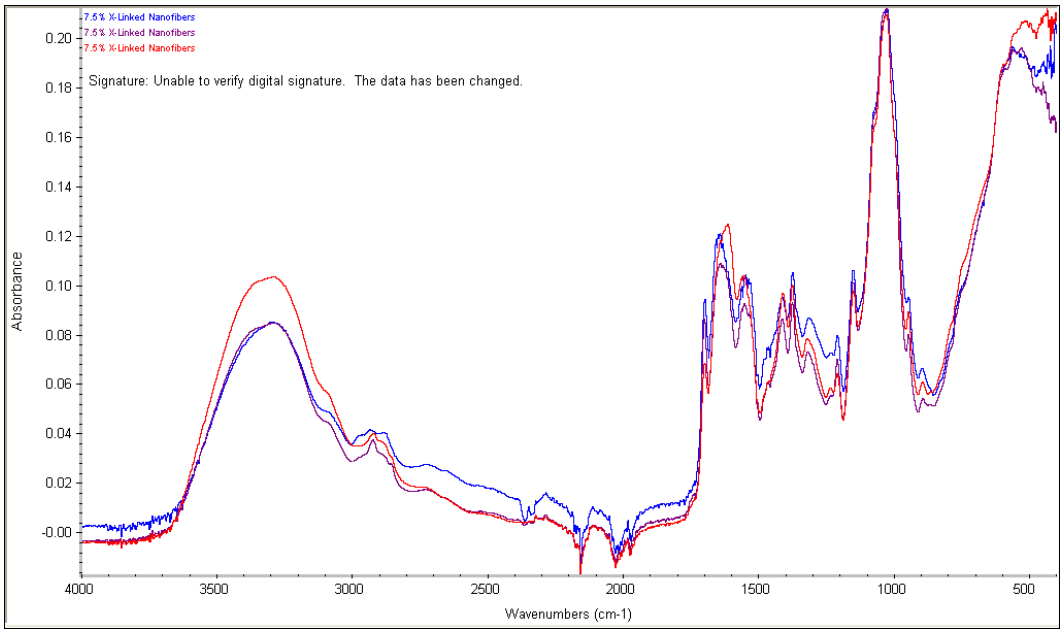

Figure 5.3: FT-IR scan of 7.5% crosslinked nanofiber meshes

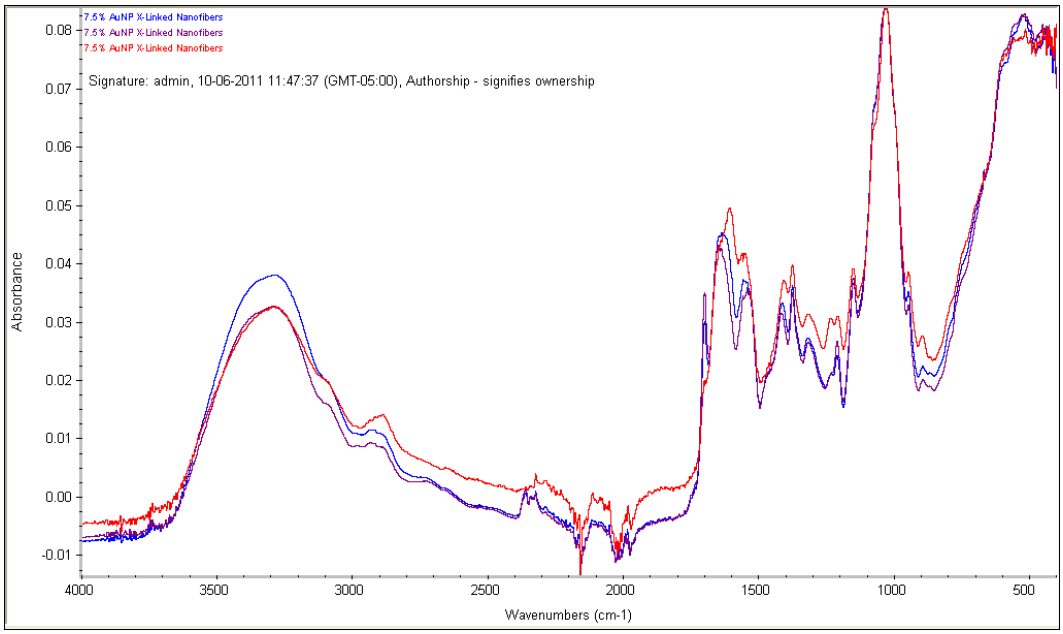

Figure 5.4: FT-IR scan of 7.5% AuNP conjugated nanofiber meshes

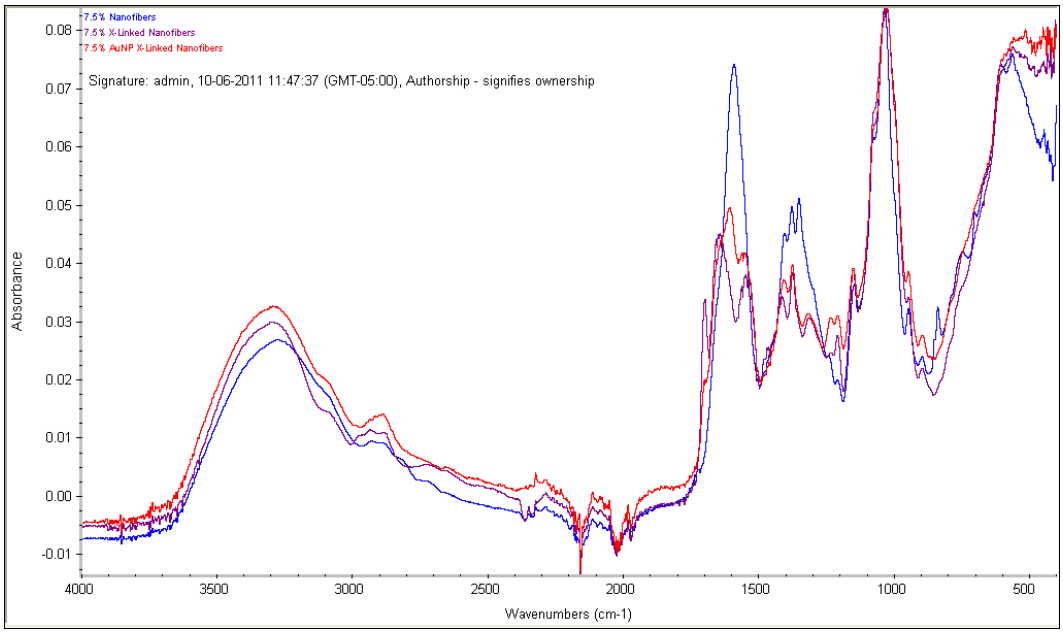

Figure 5.5: FT-IR scan of 7.5% nanofiber mesh (blue), crosslinked nanofiber mesh (purple), and AuNP conjugated nanofiber mesh (red)

5.3.2. Analysis of Crosslinked Nanofibers Using SEM/EDS

Backscatter electron SEM was utilized to analyze the morphology of the nanofiber meshes after crosslinking and AuNP conjugation. Figure 5.6 shows the SEM image of the HA/collagen scaffold after the crosslinking procedure was performed. The figure shows that the nanofibers are less well defined, but still visible. This is may be due to the EDC binding to the different groups on the mesh surface so as to render the mesh insoluble. The small holes in the mesh are a result of the electron beam. The meshes are soft and have low denaturation temperatures, so the powerful electron beam was burning holes in the meshes very quickly during this analysis.

An SEM image of the mesh after AuNP conjugation can be seen in Figure 5.7. The individual nanofibers can still be seen, but are less visible than in the crosslinked mesh image. Additionally, there are some holes from the strong electron beam. The significance of this image is the presence of charged particles that appear as brighter

spots on the image. This is an initial indication that the AuNPs have attached to the mesh surface.

EDS was then utilized to determine the composition of the charged particles from the SEM image and to confirm the presence of gold. Figure 5.8 shows the elemental analysis of selected charged particles on the mesh surface. The presence of gold is confirmed by the peak at 2.14 keV in the EDS spectrum of point 1. The presence of the Aluminum peak is not alarming because the meshes are mounted on an aluminum surface. This is because the aluminum foil containing the nanofiber meshes was mounted onto a tacky stage that is inserted into the SEM before imaging.

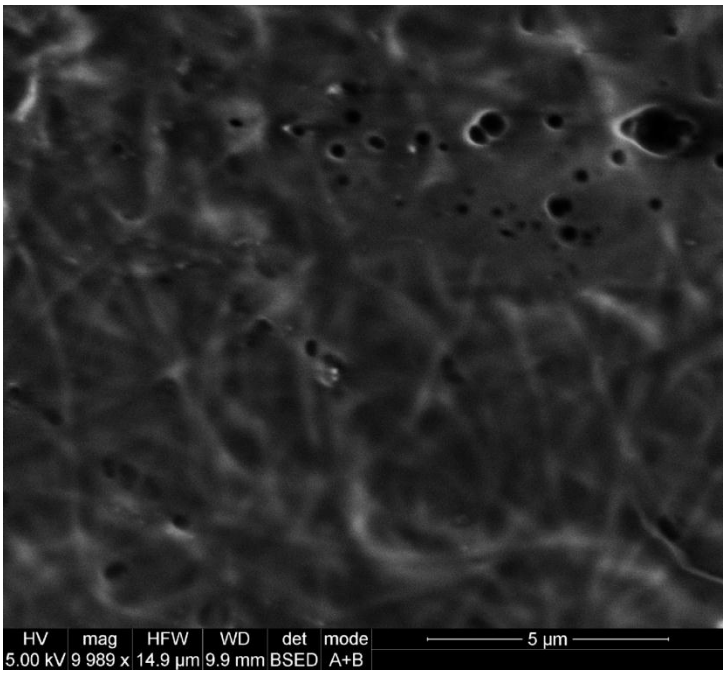

Figure 5.6: SEM image of HA/collagen scaffold after crosslinking

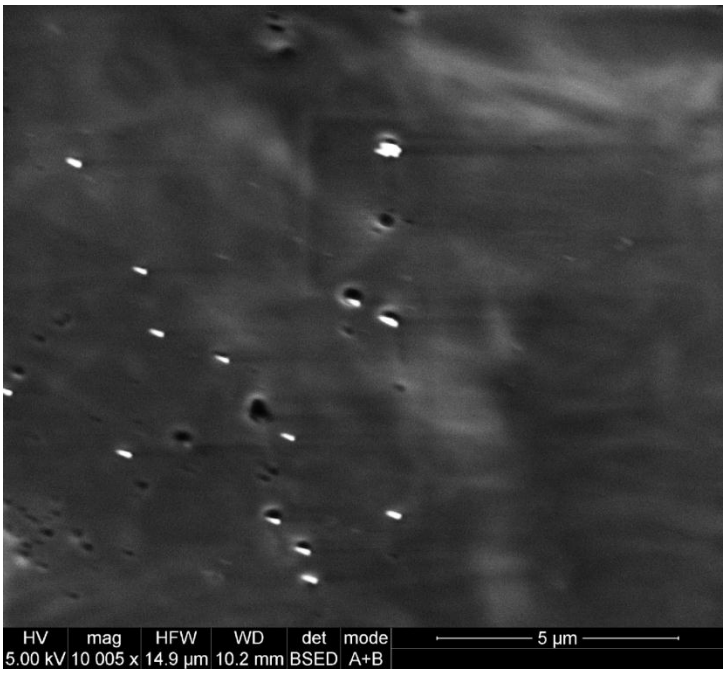

Figure 5.7: SEM image of HA/collagen nanofibers after AuNP conjugation

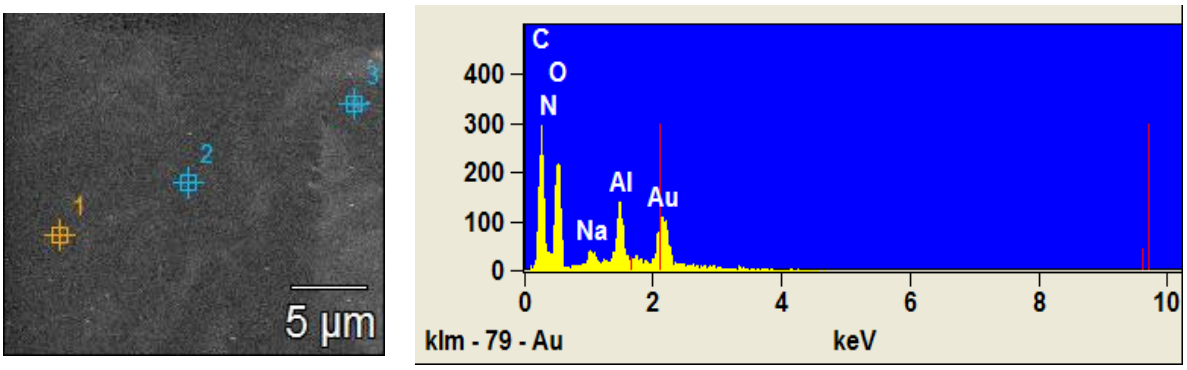

Figure 5.8: EDS analysis for point 1 selected on the SEM image of 7.5% nanofiber meshes conjugated with AuNPs

5.4. Conclusion

After experimentation the optimal EDC crosslinking and AuNP conjugation protocol was determined. Since HA is soluble in aqueous medium this crosslinking was required before additional testing could be performed. Initial testing used 5 mM EDC in 95% ethanol and did not sufficiently crosslink the mesh surfaces so they continued to dissolve during the PBS rinse. After additional research was performed to determine what other crosslinking methods have been tested, it was found that many different EDC concentrations, ethanol concentrations, and crosslinking time frames can be utilized. From an optimization study comparing many of these variables, it was determined that 50 mM EDC in 95% ethanol for 22 hours created adequately crosslinked scaffolds that retained their original shape and color. After crosslinking, AuNPs were conjugated to the mesh surface. The finalized crosslinking and AuNP conjugation protocol can be seen in Appendix 2.

Additional testing was performed to characterize these processing steps. FT-IR was conducted to determine the functional group changes after each processing step. This showed the changes that were made during the crosslinking and subsequent AuNP conjugation by differences in the absorption spectrums. SEM images were then taken to view the morphological changes after each processing step. This showed how the nanofibers changed throughout the processing. EDS was then used to confirm the charged particles on the mesh were gold. After crosslinking, in order to render the meshes insoluble, and gold nanoparticles conjugation, cell studies were performed. This was done on both crosslinked meshes and AuNP conjugated meshes to determine the potential biocompatibility of the meshes and to determine if the AuNPs increase biocompatibility.

CHAPTER 6
INVESTIGATION OF CELLULARITY

6.1. Introduction

As discussed in the literature review in Chapter 2 gold nanoparticles have properties that make them suitable for biological applications. In this experiment, gold nanoparticles were added to HA/collagen nanofiber meshes to stimulate cells to promote bone growth in osteoporosis patients (Gu et al. 2009). This investigation aims to test the cellularity of the HA/collagen crosslinked meshes and the HA/collagen AuNP conjugated meshes for potential use as implantable biomaterials.

The cell response of the meshes was tested using a continuous line of murine fibroblast cells (L929). This cell line was selected based on its sensitivity that was demonstrated in cytotoxicity testing (Thonemann et al. 2002). In this experiment, a water soluble tetrazolium (WST-1) assay (Roche Diagnostics, Indianapolis, IN) was used to measure the cell response of L929 fibroblasts grown in well plates with the HA/collagen crosslinked and HA/collagen AuNP conjugated scaffolds. This assay was based on the reduction of WST-1 by viable cells. In the presence of viable cells, the WST-1 is reduced to a formazan dye by glycolic production of NADPH. The cells are grown on the meshes for three days before the assay is conducted. After the assay was run, quantitating the absorption of formazan dye directly correlates to the viable cell number. This assay was selected based on its effectiveness and positive results that have been shown by other studies performed in the Biosensors and Biomaterials Laboratory on AuNP conjugated tissue engineered materials (Cozad et al. 2011).

6.2. Materials and Methods

6.2.1. Preparation of Nanofiber Meshes

In order to perform the WST-1 assay the nanofiber meshes needed to be sterilized. During the sterilization and during all of the cell culture procedures aseptic techniques were followed and containers holding the cells were only opened in the sterile environment. To begin sterilization, the 48-well plate containing the meshes in the 70% ethanol was transferred into the biologic hood. Meshes were then transferred to a new, sterile, 24-well plate in preparation for the WST-1 assay. There were four different test groups, in addition to a blank control, that are outlined in Table 6.1. The well-plate layout can be seen in Table 6.2. The four different groups are 1) 'AuNP cells' that had meshes that were crosslinked and conjugated with the gold nanoparticles where cells will be added in subsequent steps, 2) 'AuNP' that had meshes that were crosslinked and conjugated with the gold nanoparticles, 3) 'XL cells' that had meshes that were crosslinked where cells will be added in subsequent steps, and 4) 'XL' that had meshes that were crosslinked.

Table 6.1: Sample size for WST-1 assay

	# of Samples		
Experimental Groups	**W/ Cells**	**W/O Cells**	**Total**
No Scaffold (Controls)		1 (Blank)	1
X-linked	9	2	11
X-linked AuNP	10	2	12
Individual Totals	**19**	**5**	
Overall Total	**24**		

Table 6.2: WST-1 Assay 24-well plate layout

	1	2	3	4	5	6
A	AuNP cells	AuNP cells	AuNP cells	AuNP cells	AuNP cells	AuNP cells
B	AuNP cells	AuNP cells	AuNP cells	AuNP cells	AuNP	AuNP
C	XL cells	XL cells	XL cells	XL cells	XL cells	XL cells
D	XL cells	XL cells	XL cells	XL	XL	Blank

The meshes were sterilized by adding 0.5 mL of 70% ethanol into each well for 15 minutes. The ethanol was then removed and 0.5 mL of sterile 1X PBS was added to each well for 15 minutes to remove any residual ethanol that is toxic to the cells. The PBS was then removed and 0.5 mL of cell culture medium was added to each well, including the 'Blank' and the entire well-plate was incubated at 37°C and 5% CO_2 for 24 hours. This allowed the culture medium to penetrate the meshes prior to the cells being added. The cell culture medium was ATCC-formulated Eagle's Minimum Essential Medium (Cat # 30-2003) supplemented with 10% (v/v) horse serum and PennStrep (200 U/mL) (American Type Culture Collection, Manassas, VA).

6.2.2. Preparation of Cell Culture

In order to begin this study, a sufficient number of cells needed to be prepared and readily available. There is a stock line of L929 fibroblasts cells that are continuously grown in plastic tissue culture flasks available in the Biosensors and Biomaterials Laboratory. These cells are sub-cultured on a regular basis when the cells in the flask become sub-confluent. They are stored in a prepared culture medium described previously.

To subculture the cells for the WST-1 assay, the cell culture medium was removed from the flask and the cell surface was washed with 5 mL Dulbecco's phosphate buffered saline (DTBS) without calcium and magnesium (ATCC, Manassas, VA). Then, 0.5 mL of Trypsin was then added to the flask to release the cells from the flask surface and 10 mL of new culture medium was added to suspend the cells. The fluid was then transferred to a 15 mL centrifuge tube and centrifuged at 1250 rmp for 7 minutes. Next, 8 mL of the culture medium was removed from the tube, making sure not to disturb the cells in the tube that appeared as a white line on the bottom side of the tube. Lastly, 4 mL of new culture medium was added to re-suspend the cells and to make a 6 mL solution.

A small portion of the 6 mL cell suspension was used for a counting procedure so the solution could be diluted to $3x10^{-4}$ cells/mL, which was the needed concentration for the WST-assay. To count the cells, 15 µL of the new cell suspension solution was removed and mixed with 15 µL of trypan blue (Sigma Aldrich, St. Louis, MO). The trypan blue stains live cells so they can be easily identified under a microscope. The solution was then loaded into the counting chambers of a hemacytometer. Approximately 10 µL of fluid can be loaded into each side of the chamber. After counting, the cell concentration was calculated and diluted to the desired amount of $3x10^{-4}$ cells/mL which was the cell number utilized for the WST assay. The cells were then ready to be placed in the 24-well plates.

After 24 hour incubation, the 24-well plate with the prepared meshes was removed from the incubator and transferred into the biologic hood. The culture medium in the wells containing meshes was removed, leaving the medium in the 'Blank' well alone. One mL of the properly concentrated cell suspension was then added to each well labeled with 'cells' (Table 6.2) and 1 mL of fresh culture medium was added to the

wells without cells. The well-plate was then transferred back into the incubator for 48 hours. After 48 hours, 0.5 mL of the culture medium was removed from all wells except the ‘Blank’ well and replaced with0.5 mL of fresh culture medium. The well-plate was then incubated for 24 more hours.

6.2.3. Incubation of Cells and Meshes with WST-1

After the cells were exposed to the meshes for the proper duration of time, the WST-1 reagent was used to evaluate the cell response from each mesh group. The protocol was adapted from Cozad et al. (2011). The well plate was removed from the incubator and 0.5 mL of the culture medium was removed from all wells except the ‘Blank’ well. This left all of the wells with 0.5 mL of solution. The WST-1 reagent was thawed in a water bath before use. Once thawed, 50 µL of the reagent was added to each well, including ‘blank’ to create a 1:10 ratio of WST-1 to cell solution. The well plate was then moved back to the incubator while the reaction occurred. For this assay, absorbance was run after two hours and after three hours. These time points were determined from a previous assay that was conducted over four hours that resulted in over saturation and did not produce any results.

6.2.4. Quantification of WST-1 Assay

At each time point the viability of the cells exposed to the meshes was quantified by measuring the absorbance of the formazan dye in each well. To measure the absorbance, 100 µL of the solution from each well and the ‘Blank’ well was moved to a corresponding well in a 96-well microplate. The absorbance was then read by a Bio-Rad Model 680 Microplate Reader (Bio-Rad Laboratories, Hercules, CA) and data was interpreted by Microplate Manager Software, version 5.2.1. The blank absorbance was

subtracted from the total absorbance from each well to account for any absorbance from the culture medium that was not attributed to cellularity. The wells with meshes only and no cells were tested to verify that there was no formazan dye in wells that were not supposed to have cells.

6.2.5. Statistical Analysis

Statistical analysis was performed to compare absorbance readings from the WST-1 assay. All statistical analysis was performed using GraphPad Prism® software, version 4.0. An unpaired t-test with a 95% confidence interval was utilized to determine significant differences between the experimental means. Experiments with P-Values greater than 0.05 indicated that the means were not significantly different.

6.3. Results and Discussion

Initially, a small scale WST-1 assay was performed to obtain a general idea of the cellular response. Two different mesh types were tested: crosslinked and gold nanoparticle conjugated. In both cases, the meshes were exposed to cells for 3 days. The initial absorbance reading was taken after four hours of incubation and several of the wells were oversaturated so the microplate reader could not obtain values. From the values that were obtained, the results showed cellular activity in both mesh types, but due to the small scale, no statistical analysis could be performed.

From this, a larger test was developed for the same two mesh types that would run for 3 days and test for absorbance at two and three hours. The shorter incubation times would insure that the samples did not become oversaturated. Recent studies have shown increased biocompatibility in AuNP conjugated materials, including polyethelene terephthalate and acellular tissue (Cozad et al. 2011; Whelove 2010). This WST-1 assay

helped determine if the AuNP conjugated meshes had increased cellularity which would indicate potential increased biocompatibility. Table 6.3 shows a summary of the WST-1 Assay results for the different mesh types at the two time periods. Figure 6.1 shows a graph representing the same data. The red bracket represents the standard deviation and the solid red line represents the data mean. It is clear that both mesh types promoted cellular growth, which demonstrated that the meshes are biocompatible and non-toxic to cells, and that the processing parameters allowed cells to attach and readily proliferate. Appendix 5 shows a complete summary of the absorption results including a confirmation that the wells that did not have cells did not produce the formazan dye.

Statistical analysis was performed to determine if there was a difference in cellularity between the mesh types at the two different time points. The t-test comparing the two types of meshes had a P-value of 0.4541 at two hours and a value of 0.3033 at three hours. Since both values are greater than 0.05, there was no significant difference in the means, indicating that the data was comparable. This test did not definitively show that the AuNP had a biocompatible advantage to the crosslinked mesh, but it did show that there are no cytotoxic effects. More testing should be performed to determine if the AuNPs show enhanced biocompatibility.

Table 6.3: Summary of WST-1 assay results

Mesh #	2 hrs		3 hrs	
	AuNP Cells	XL Cells	AuNP Cells	XL Cells
1	0.99	1.251	0.582	0.639
2	0.631	1.204	0.466	0.61
3	0.611	0.88	0.413	0.511
4	0.787	0.827	0.721	0.443
5	0.853	0.895	0.486	0.428
6	1.167	0.927	0.525	0.273
7	0.489	1.138	0.249	0.632
8	0.542	0.932	0.56	0.457
9	1.606	1.616	0.883	0.554
10	1.452		0.707	
Average	0.913	1.074	0.559	0.505
Standard Dev.	0.387	0.255	0.178	0.119

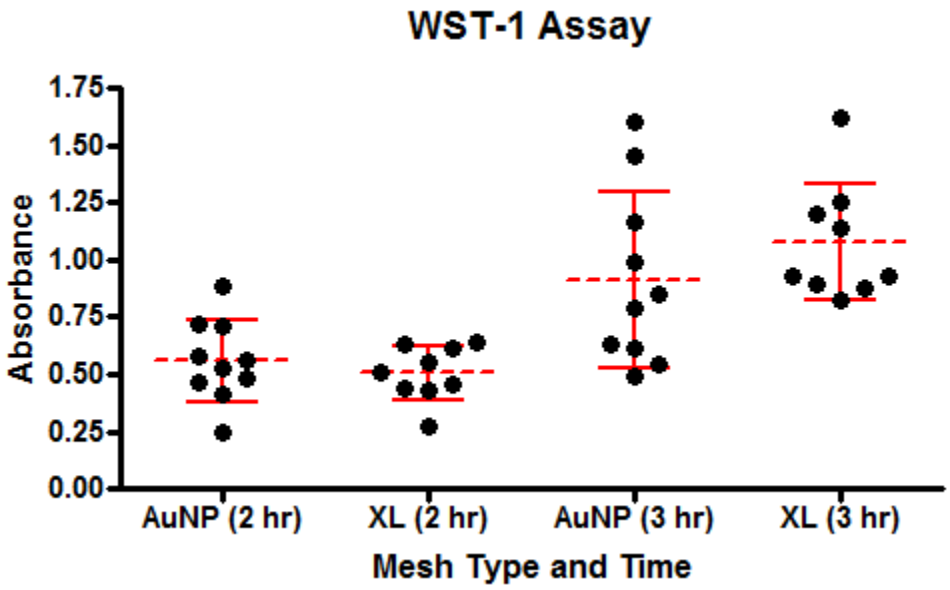

Figure 6.1: WST-1 Assay Absorbance Graph

6.4. Conclusion

The WST-1 assay was performed to determine the potential cellularity of the collagen/HA meshes and gold nanoparticle conjugated collagen/HA meshes. The complete protocol can be seen in Appendix 3. Other studies have shown the presence of AuNPs can increase cellularity of a material, which is optimal for increased biocompatibility and the integration of cells into tissue engineered materials. This assay exposed cells to the meshes for three days to determine cell attachment and growth as well as the effects of gold nanoparticles.

The results show that the AuNPs do not have a cytotoxic effect on the meshes during the three day exposure. The results also show a similar response to the cells in both of the mesh types that were tested. This study did not show AuNP conjugated meshes to have increased cellularity to the crosslinked meshes, but it did provide valuable evidence to their non-toxic effects. Additional assays can be performed to better quantify the biocompatible nature of these meshes.

CHAPTER 7
FUTURE WORK

7.1. Introduction

The work presented here designed protocols to electrospin a uniform hyaluronic acid and collagen nanofiber mesh material to be used in tissue engineering. Processing steps were also developed to crosslink the collagen/HA material rendering them insoluble in aqueous solutions, which also allowed conjugation of gold nanoparticles to the mesh surface. FT-IR testing was performed throughout the process to confirm the surface modification of the mesh. SEM and EDS imaging was conducted to verify the presence of gold on the mesh surface and view the morphological structure of the material. A WST-1 assay was conducted to demonstrate the biocompatibility of the collagen/HA mesh materials and that AuNPs were not toxic to cells. From these studies, there are several paths for future research.

7.2. Additional Testing

Additional testing can be conducted to determine the potential anti-microbial effects these meshes may have. In addition to gold being non-toxic and promoting cellularity, AuNPs have also been shown to be anti-microbial. If these meshes are anti-microbial it could be a benefit in procedures where infection is sometimes present. Bacteria studies can be performed to determine the meshes response to different bacteria types and weather the presence of the AuNPs will prevent bacterial adhesion. In the presence of bacteria, the AuNP conjugated meshes may be able to minimize the bacterial growth. Additionally, gold nanoparticles have been reported to be electron

scavengers. Thus, a reactive oxygen species (ROS) assay could be conducted to determine if these meshes can scavenge free radicals that cause enhanced inflammation. By minimizing ROS production, would healing would proceed at a faster rate.

7.3. Electrospinning Parameter Modifications

There could also electrospinning parameter modifications during the fabrication of these mesh materials. One change would be to lay the electrospinning device on its side so the polymer jet is parallel to the ground. Then the counter electrode would not be directly under the tip, which would eliminate the effects of dripping, distort the structure of the mesh. This method has been utilized successfully for hyaluronic acid polymer solution (Ji et al. 2006). This processing method could also extend the working time of the polymer fluid because a more viscous solution could be, as long as nanofibers are still being produced and deposited onto the counter electrode. The processing method could also help generate thicker meshes. Once a thicker mesh is developed Instron testing could be performed to assess the mechanical strength of the device.

The electrospinning process could also be aided by a mandrel that would help align the nanofibers. Kim and Park (2006) used this method to electrospin poly-lactic-co-glycolic acid blended with polycaprolactone. Their device used a rotating drum at 500 mm/s as opposed to the more stationary common ground plate (Kim and Park 2006). The SEM images from this study still show a random orientation of nanofibers, but this processing method could create mesh tubes that could have multiple layers depending on the desired function. Other processing techniques could be used to generate more aligned nanofiber meshes. Instead of a mandrel, Rafique et al. (2007) used a method that ejects polycaprolactone and polyacrylonitrile polymer fibers one by one. Once a

single fiber is deposited the next fiber is repelled by the former fiber when it moves towards the collector which causes it to arrange itself parallel to the former one (Rafique et al. 2007). Similar techniques could be used with HA/collagen to generate different mesh morphologies.

7.4. *In-Vivo* Studies

In-vivo animal studies could also be performed to determine the degradation rate of this device in its desired application for increasing bone strength. The mesh could be implanted into the bones on animals and studied at different time points to determine the effects. This would help assess the degradation rate of the device, if it promotes the growth of stronger bone, and if it allows cell infiltration without causing an inflammatory response.

APPENDIX 1

ELECTROSPINNING HYALURONIC ACID AND COLLAGEN PROTOCOL

Chemicals:

- Hyaluronic acid (HA) (Lifecore Biomedical, Chaska, MN)
- Collage type I from calf skin (Sigma Aldrich, St. Louis, MO)
- Sodium hydroxide (NaOH)
- Dimethyl formamide (DMF)

Materials:

- TYGON Tubing
- Male and female hose barbs
- 20 gauge needle
- 3 mL syringe

Procedure:

Makes 2 mL of 7.5 % wt/vol Hyaluronic acid/collagen (95/5 weight ratio)

1. Make a 0.5 M solution of NaOH.

2. Combine 1.6 mL NaOH with 0.0075 g collagen and let sit overnight.

3. Add 0.4 mL DMF and 0.1425 g HA to the NaOH/collagen mixture

4. Vortex the solution until the HA is dissolved (No more than 5 minutes). Every minute stop mixing and stir with metal stirrer to make sure the HA becomes incorporated.

5. Transfer the solution into a 3 mL syringe.

6. Using the TYGON tubing and hose barbs connect the syringe to a 20 gauge needle. Place the syringe in the syringe pump and place the needle in the holder in the Plexiglas box.

7. Begin to electrospin using the following apparatus parameters.

    - Voltage: 16 kV
    - Plate Separation: 5 cm
    - Flow Rate: 10 µL/min
    - Ground Plate: 2 in^2 Aluminum foil piece

8. Collect the nanofibers for about 10 minutes, or until a uniform nanofiber mesh is created.

- Monitor voltage and flow rate continually to make sure the solution does not drip onto the foil. Make adjustments as needed.
- The goal is to have a polymer solution drop suspended at the end of the needle tip. The nanofiber formation should be visible when fiber formation is in progress.

9. Turn off voltage and replace aluminum foil piece.

10. Continue to make new scaffolds until the solution becomes too viscous to electrospin, about one hour.

11. Collect and store scaffolds until additional processing is needed.

APPENDIX 2

CROSSLINKING AND GOLD NANOPARTICLE CONJUGATION PROTOCOL

Crosslinking:

1. Remove nanofiber meshes from aluminum foil squares carefully, making sure not to tear or crumple them.
2. Cut mesh into 4.8 mm diameter circles and place individually into a 48-well plate
3. Make a solution of 50 mM EDC in 95% ethanol.
4. Pipette 0.5 mL of solution into each well and let sit for 22 hours.
5. Remove ethanol solution.
6. For scaffolds that are just being crosslinked add 70% ethanol to the wells for storage. For the scaffolds that are being conjugated with AuNPs continue to the following AuNP conjugation.

AuNP Conjugation:

1. For each batch, make a solution with 4 mg EDC, 5.3 mg NHS, and 0.25 mL dH_2O. Count up number of wells for conjugation and multiply components accordingly to make one solution. (Each batch fills 2 wells)
2. Pipette 0.125 mL of the solution in to each well and let sit for a few minutes.
3. Pipette 0.125 mL 100 nm AuNPs into each well and let sit for one hour.
4. Pipette off all solution.
5. Pipette 0.5 mL 70% ethanol into each well for storage.

   * If the scaffolds do not remain wet, they will stick to the bottom of the well and can no longer be used. Because of this they should be stored in 70% ethanol until they are needed for additional testing.

APPENDIX 3

CELL VIABILITY (WST-1) PROTOCOL

	# of Samples		
Experimental Groups	**W/ Cells**	**W/O Cells**	**Total**
No Scaffold (Controls)		1 (Blank)	1
X-linked	9	2	11
X-linked AuNP	10	2	12
Individual Totals	**19**	**5**	
Overall Total	**24**		

1. After sterilizing biological hood and allowing it to run for at least 30 minutes, place needed and sterilized supplies in the hood.

2. Using BD Falcon cell culture-treated 24-well plates (see following layout), place one mesh per well as depicted.

	1	2	3	4	5	6
A	AuNP cells	AuNP cells	AuNP cells	AuNP cells	AuNP cells	AuNP cells
B	AuNP cells	AuNP cells	AuNP cells	AuNP cells	AuNP	AuNP
C	XL cells	XL cells	XL cells	XL cells	XL cells	XL cells
D	XL cells	XL cells	XL cells	XL	XL	Blank

24-well plate layout. Wells without cells have scaffolds and culture medium only, no cells, which will serve as controls. The blank is a well with culture medium only. (AuNP= HA/collagen AuNP conjugated, XL= HA/collagen crosslinked)

3. Add 0.5 mL 70% ethanol into each occupied well and let stand for 15 minutes to sterilize.

4. Remove ethanol from wells.

5. Add 0.5 mL 1X PBS into each occupied well for 15 minutes to rinse ethanol (ethanol is toxic to the cells).

6. Remove PBS from wells.

7. Add 0.5 mL of cell culture medium (ATCC-formulated Eagle's Minimum Essential Medium (Cat # 30-2003) supplemented with 10% (v/v) horse serum and PennStrep (200 U/mL)) into each well, including 'Blank'. Place in incubator at 37 °C and 5% CO_2 for 24 hours.

8. Remove L929 murine fibroblast cells from the culture flask, centrifuge, suspend in fresh culture medium, and count them using the hemacytometer. Dilute these cells to a concentration of 3×10^4 cells/mL.

9. Remove culture medium from wells containing scaffolds. Leave medium in 'Blank' well.

10. Add 1 mL of cell suspension to each well labeled with 'cells' and add 1 mL of culture medium to each well without cells. Place well-plate in incubator at 37 °C and 5% CO_2 for 2 days.

11. After sterilizing biological hood and allowing it to run for at least 30 minutes, remove culture plates from incubator. Remove 0.5mL of culture medium from each well and replace with 0.5 mL of fresh culture medium. Place plates back in incubator at 37 °C and 5% CO_2 for 1 day.

12. After sterilizing biological hood and allowing it to run for at least 30 minutes, remove plates from incubator, withdraw 0.5 mL of cell media from each well, and add 50 µL of WST-1 to each well and incubate for 3 hours.

13. Remove 100 µL of media from each well and place in separate wells of a 96-well microplate.

	1	2	3	4	5	6	7	8	9	10	11	12
A	AuNP cells	AuNP cells	AuNP cells	AuNP cells	AuNP cells	AuNP cells						
B	AuNP cells	AuNP cells	AuNP cells	AuNP cells	AuNP	AuNP						
C	XL cells	XL cells	XL cells	XL cells	XL cells	XL cells						
D	XL cells	XL cells	XL cells	XL	XL							
E												
F												
G												
H												Blank

Microplate 96 well Template. Wells are filled with solution from the corresponding well on from the 24-well plate. The 'Blank' is a well with culture medium and WST-1 only.

14. Turn on the BioRad 680 Microplate Reader using switch on back right side. After allowing it to warm up for ~ 1 minute, press '0' five times and then press enter.

15. Slide the door back on the microplate reader and snap the 96-well plate into place. Also, be sure to leave the lid off of the 96-well plate.

16. Close lid on reader, go to the computer, and open Microplate Manager.

17. Go to File->Open. Under file type at the bottom of the new window select Endpoint Protocol and then select 'WST-1 Assay 09-27-10' from the window.

18. An endpoint protocol should load with the following parameters:

    a. Fast read.

    b. Medium mix speed for 10 seconds.

    c. Absorbance measurement reading at 450 nm with 655 nm reference reading using subtraction of the reference wavelength.

19. Click "Show template and make sure the template matches the setup of your 96-well microplate. If not, use the toolbar at the top to select wells as unknowns, standard, or blanks.

20. Click Run to begin the reading.

21. When the reading is done, click File->SaveData/Template to save all the Microplate Manager Data files. Also, select each spreadsheet window individually and click File->Export and save the files as .csv type.

22. Shut down the program and reader and dispose of your samples.

APPENDIX 4

NANOFIBER DIAMETER DATA

Table A.1: Rachael's diameter data

	5% 95/5	5% 80/20	7.5% 95/5
1	140	202	395
2	233	126	257
3	186	119	286
4	233	80	352
5	110	155	257
6	110	177	285
7	208	135	298
8	139	119	286
9	160	109	351
10	155	112	219
11	147	151	312
12	133	80	186
13	140	188	312
14	175	210	175
15	132	155	324
16	158	135	343
17	110	137	307
18	187	101	233
19	181	101	286
20	110	80	281
Average	157.35	133.6	287.25
Standard dev.	38.28188	38.99582	36.66674

Table A.2: Michael's diameter data

	5% 95/5	5% 80/20	7.5% 95/5
1	127	165	379
2	108	146	373
3	230	106	293
4	119	183	301
5	101	155	324
6	138	157	438
7	213	158	586
8	73	149	230
9	101	134	321
10	196	105	429
11	140	152	443
12	186	58	146
13	91	161	466
14	88	117	541
15	189	203	114
16	67	106	258
17	135	118	366
18	112	150	183
19	88	161	474
20	185	219	433
Average	134.35	145.15	354.9
Standard dev.	48.98149	36.66674	127.09503

APPENDIX 5

WST-1 ASSAY DATA

Table A.3: WST-1 assay two hour data

	2 hours			
Mesh #	**AuNP Cells**	**AuNP**	**XL Cells**	**XL**
1	0.99	-0.014	1.251	-0.018
2	0.631	-0.011	1.204	-0.018
3	0.611		0.88	
4	0.787		0.827	
5	0.853		0.895	
6	1.167		0.927	
7	0.489		1.138	
8	0.542		0.932	
9	1.606		1.616	
10	1.452			
Average	0.913	-0.013	1.074	-0.018
Standard Dev.	0.387	0.002	0.255	0.000

Table A.4: WST-1 assay three hour data

	3 hours			
Mesh #	**AuNP Cells**	**AuNP**	**XL Cells**	**XL**
1	0.582	-0.092	0.639	0.009
2	0.466	-0.009	0.61	-0.016
3	0.413		0.511	
4	0.721		0.443	
5	0.486		0.428	
6	0.525		0.273	
7	0.249		0.632	
8	0.56		0.457	
9	0.883		0.554	
10	0.707			
Average	0.559	-0.051	0.505	-0.004
Standard Dev.	0.178	0.059	0.119	0.018

REFERENCES

Bai, J., Li, Y., Yang, S., Du, J., Wang, S., Zheng, J., Wang Y, Yang Q, Chen X, Jing, X. (2007). A simple and effective route for the preparation of poly(vinylalcohol) (PVA) nanofibers containing gold nanoparticles by electrospinning method. *Solid State Communications, 141*(5), 292-295.

Barnes, C. P., Pemble IV, C. W., Brand, D. D., Simpson, D. G., and Bowlin, G. L. (2007). Cross-linking electrospun type II collagen tissue engineering scaffolds with carbodiimide in ethanol. *Tissue Engineering, 13*(7), 1593-1605.

Bartel, D. L., Davy, D. T., and Keaveny, T. M. (2006). *Orthopaedic Biomechanics: Mechanics and Design in Muskuloskeletal Systems* Pearson Education. 9-20, 73-78.

Boskey, A., and Camacho, N. P. (2007). FT-IR imaging of native and tissue- engineered bone and cartilage. *Biomaterials, 28*(15), 2465-2478.

Camacho, N. P., West, P., Torzilli, P. A., and Mendelsohn, R. (2001). FTIR microscopic imaging of collagen and proteoglycan in bovine cartilage. *Biopolymers, 62*(1), 1-8.

Chang, M. C., and Tanaka, J. (2002). FT-IR study for hydroxyapatite/collagen nanocomposite cross-linked by glutaraldehyde. *Biomaterials, 23*(24), 4811-4818.

Chemblink. (2011). Online Database of Chemicals From Around the World. Retrieved 10/08/2011, from www.chemblink.com

Cleland, J. G. F., Witte, K., and Steel, S. (2010). Calcium supplements in people with osteoporosis. *BMJ, 341*(7767), 260-261.

Cozad, M. J., Bachman, S. L., and Grant, S. A. (2011). Assessment of decellularized porcine diaphragm conjugated with gold nanomaterials as a tissue scaffold for wound healing. *Journal of Biomedical Materials Research Part A, 99A*(3), 426-434.

Cui, W., Li, X., Zhou, S., and Weng, J. (2007). Investigation on process parameters of electrospinning system through orthogonal experimental design. *Journal of Applied Polymer Science, 103*(5), 3105-3112.

Deeken, C. R., Fox, D. B., Bachman, S. L., Ramshaw, B. J., and Grant, S. A. (2011). Characterization of bonanocomposite scaffolds comprised on amine-functionalized gold nanoparticles and silicon carbide nanowires crosslinked to an acellular porcine tendon. *Journal of Biomedical Materials Research - Part B Applied Biomaterials, 97 B*(2), 334-344.

Formhals, A. (1934). Process and apparatus for preparing artificial threads. vol. 1,975,504. United States Patent Office.

Garg, K., and Bowlin, G. (2011). Electrospinning jets and nanofibrous structures. *Biomicrofluidics, 5*(1), 1-19.

Gauthier, A., Kanis, J. A., Martin, M., Compston, J., Borgström, F., Cooper, C., and McCloskey, E. (2011). Development and validation of a disease model for postmenopausal osteoporosis. *Osteoporosis International, 22*(3), 771-780.

Greiner, A., Wendorff, J. H., Yarin, A. L., and Zussman, E. (2006). Biohybrid nanosystems with polymer nanofibers and nanotubes. *Applied Microbiology and Biotechnology, 71*(4), 387-393.

Gu, Y.-J., Cheng, J., Lin, C.-C., Lam, Y. W., Cheng, S. H., and Wong, W.-T. (2009). Nuclear penetration of surface functionalized gold nanoparticles. *Toxicology and Applied Pharmacology, 237*(2), 196-204.

He, W., Ma, Z., Yong, T., Teo, W. E., and Ramakrishna, S. (2005). Fabrication of collagen-coated biodegradable polymer nanofiber mesh and its potential for endothelial cells growth. *Biomaterials, 26*(36), 7606-7615.

Homenick, C. M., Sheardown, H., and Adronov, A. (2010). Reinforcement of collagen with covalently-functionalized single-walled carbon nanotube crosslinkers. *Journal of Materials Chemistry, 20*(14), 2887-2894.

Hosoi, T. (2010). Genetic aspects of osteoporosis. *Journal of Bone and Mineral Metabolism, 28*(6), 601-607.

Hsu, F. Y., Hung, Y. S., Liou, H. M., and Shen, C. H. (2010). Electrospun hyaluronate-collagen nanofibrous matrix and the effects of varying the concentration of hyaluronate on the characteristics of foreskin fibroblast cells. *Acta Biomaterialia, 6*(6), 2140-2147.

Ji, Y., Ghosh, K., Shu, X. Z., Li, B., Sokolov, J. C., Prestwich, G. D., Clark R.A.F. Rafailovich, M. H. (2006). Electrospun three-dimensional hyaluronic acid nanofibrous scaffolds. *Biomaterials, 27*(20), 3782-3792.

Johnell, O., and Kanis, J. A. (2006). An estimate of the worldwide prevalence and disability associated with osteoporotic fractures. *Osteoporosis International, 17*(12), 1726-1733.

Jose, M. V., Thomas, V., Dean, D. R., and Nyairo, E. (2009). Fabrication and characterization of aligned nanofibrous PLGA/Collagen blends as bone tissue scaffolds. *Polymer, 50*(15), 3778-3785.

Kaveh, K., Ibrahim, R., Emadi, M., Bakar, M. Z. A., and Ibrahim, T. A. (2010). Osteoporosis and bone health. *Journal of Animal and Veterinary Advances, 9*(6), 1048-1054.

Kim, T. G., Chung, H. J., and Park, T. G. (2008). Macroporous and nanofibrous hyaluronic acid/collagen hybrid scaffold fabricated by concurrent electrospinning and deposition/leaching of salt particles. *Acta Biomaterialia, 4*(6), 1611-1619.

Kim, T. G., and Park, T. G. (2006). Surface functionalized electrospun biodegradable nanofibers for immobilization of bioactive molecules. *Biotechnology Progress, 22*(4), 1108-1113.

Lannutti, J., Reneker, D., Ma, T., Tomasko, D., and Farson, D. (2007). Electrospinning for tissue engineering scaffolds. *Materials Science and Engineering C, 27*(3), 504-509.

Liu, K. Z., Jackson, M., Sowa, M. G., Ju, H. S., Dixon, I. M. C., and Mantsch, H. H. (2006). Modification of the extracellular matrix following myocardial infracion monitored by FTIR spectroscopy. *Biochimica et Biophysica Acta-Molectular Basis of Disease, 1335*(2), 73-77.

Liu, Y., Ma, G., Fang, D., Xu, J., Zhang, H., and Nie, J. (2011). Effects of solution properties and electric field on the electrospinning of hyaluronic acid. *Carbohydrate Polymers, 83*(2), 1011-1015.

Lujan, B., and White, R. Human Physiology in Space. Retrieved 09/08/2011, from http://www.nsbri.org/humanphysspace/index.html

Martin, G. (1977). Fibrillar product of electrostatically spun organic material. vol. 4,043, 331. United States Patent Office.

Matthews, J. A., Wnek, G. E., Simpson, D. G., and Bowlin, G. L. (2002). Electrospinning of Collagen Nanofibers. *Biomacromolecules, 3*, 232-238.

McCombs, J. S., Thiebaud, P., McLaughlin-Miley, C., and Shi, J. (2004). Compliance with drug therapies for the treatment and prevention of osteoporosis. *Maturitas, 48*(3), 271-287.

Muyonga, J. H., Cole, C. G. B., and Duodu, K. G. (2004). Fourier transform infrared (FTIR) spectroscopic study of acid soluble collagen and gelatin from skins and bones of young and adult Nile Perch. *Food Chemistry, 86*(3), 325-332.

Park, S. N., Park, J. C., Kim, H. O., Song, M. J., and Suh, H. (2002). Characterization of porous collagen/hyaluronic acid scaffold modified by 1-ethyl-3-(3-dimethylaminopropyl)carbodiimide cross-linking. *Biomaterials, 23*(4), 1205-1212.

Pocock, N. A., Eisman, J. A., Hopper, J. L., Yeates, M. G., Sambrook, P. N., and Eberl, S. (1987). Genetic determinants of bone mass in adults: A twin study. *Journal of Clinical Investigation, 80*(3), 706-710.

Rafique, J., Yu, J., Fang, G., Wong, K. W., Zheng, Z., Ong, H. C., and Lau, W. M. (2007). Electrospinning highly aligned long polymer nanofibers on large scale by using a tip collector. *Applied Physics Letters, 91*(6).

Ramakrishna, S., Fujihara, K., Teo, W.-E., Lim, T.-C., and Ma, Z. (2005). *An Introduction to Electrospinning and Nanofibers*: World Scientific Publishing. 1-154.

Reid, I. R., Bolland, M. J., and Grey, A. (2008). Effect of calcium supplementation on hip fractures. *Osteoporosis International, 19*(8), 1119-1123.

Ritchie, R. O. (2010). How does human bone resist fracture? *Annals of the new York Academy of Sciences, 1192*, 72-80.
Seeman, E. (2008). Bone quality: The material and structural basis of bone strength. *Journal of Bone and Mineral Metabolism, 26*(1), 1-8.

Seeman, E., and Delmas, P. D. (2006). Bone quality - The material and structural basis of bone strength and fragility. *New England Journal of Medicine, 354*(21), 2250-2261.

Shin, Y. M., Hogman, M. M., Brenner, M. P., and Rutledge, G. C. (2001). Experimental characterization of electrospinning: The electrically forced jet and instabilities. *Polymer, 42*(25), 9955-9967.

Spasova, M., Stoilova, O., Manolova, N., Rashkov, I., and Altankov, G. (2007). Preparation of PLLA/PEG nanofibers by electrospinning and potential applications. *Journal of Bioactive and Compatible Polymers, 22*(1), 62-76.

Tan, W., Twomey, J., Guo, D., Madhavan, K., and Li, M. (2010). Evaluation of nanostructural, mechanical, and biological properties of collagennanotube composites. *IEEE Transactions on Nanobioscience, 9*(2), 111-120.

Thonemann, B., Schmalz, G., Hiller, K. A., and Schweikl, H. (2002). Responses of L929 mouse fibroblasts, primary and immortalized bovine dental papilla-derived cell lines to dental resin somponents. *Dental Materials, 18*(4), 218-232.

Vassalli, T. (2008). Development of electrospun synthetic bioabsorbable fibers for a novel bionanocomposite ernia repair material. *University of Missouri Master's Thesis*.

Wang, T. W., and Spector, M. (2009). Development of hyaluronic acid-based scaffolds for brain tissue engineering. *Acta Biomaterialia, 5*(7), 2371-2384.

Whelove, O. (2010). Development of gold nanoparticle conjugated polyethylene terephthalate for improved biocompatibility in hernia repair. *University of Missouri Master's Thesis*.

WHO. (1992). Assessment of fracture risk and its application to screening for postmenopausal osteoporosis. *World Health Organization Technical Reprot Series*, 1-136.

WHO. (2004). WHO scientific group on the assessment of osteoporosis at primary health care level. *World Health Organization Technical Report Series*, 1-17.